Mariana Ramos Velez

Licenciatura em Biologia Celular e Molecular

Generation of new transgenic zebrafish lines for studying neuronal circuits underlying behavior in zebrafish

Dissertação para obtenção do Grau de Mestre em
Genética Molecular e Biomedicina

Orientador: Doutora Ana Catarina Certal, Champalimaud Centre for the Unknown

Co-orientador: Doutora Ana Raquel Tomás, Champalimaud Centre for the Unknown

Júri:

Presidente: Professor Doutor José Paulo Nunes de Sousa Sampaio
Arguente: Doutor Aaron Daniel Ostrovsky

FACULDADE DE CIÊNCIAS E TECNOLOGIA
UNIVERSIDADE NOVA DE LISBOA

Setembro 2018

Faculdade de Ciências e Tecnologia da Universidade Nova de Lisboa

Mariana Ramos Velez

Licenciatura em Biologia Celular e Molecular

Generation of new transgenic zebrafish lines for studying neuronal circuits underlying behavior in zebrafish

Dissertação para obtenção do Grau de Mestre em
Genética Molecular e Biomedicina

Orientador: Doutora Ana Catarina Certal, Champalimaud Centre for the Unknown

Co-orientador: Doutora Ana Raquel Tomás, Champalimaud Centre for the Unknown

Júri:

Presidente: Professor Doutor José Paulo Nunes de Sousa Sampaio
Arguente: Doutor Aaron Daniel Ostrovsky

Setembro 2018

Generation of new transgenic zebrafish lines for studying neuronal circuits underlying behavior in zebrafish

Acknowledgments

Working at the Champalimaud Centre for the Unknown has been an incredible journey. Accomplishing this project was definitely challenging and rewarding, since it made me leave my comfort zone every day and made me grow professionally and personally. I would like to thank all the people who contributed for the final result.

First, I would like to thank Catarina Certal for the opportunity, supervision and guidance through the whole year. Thank you for all the time, trust and encouragement. It was a pleasure learning with you.

Someone without whom this would not be possible is Raquel Tomás. Thank you for the incredible mentorship, the patience and time for teaching me and making me understand how and why things are done. Thank you for all the advices, relaxing times and conversations. Thank you for helping me, supporting me and encouraging me. You are the best!

I also would like to thank Michael Orger for giving me the opportunity to develop this project and for all the orientation. Another person, that I would like to thank is Ruth Diez del Corral. Thank you Ruth for teaching me and explained me the difficult techniques and all your patience.

At the Fish Platform, all members were incredible, but I have also to thank Joana Monteiro for teaching me, helping me and supporting me. I would also like to thank Carolina Cabrera and Rita Almeida. Thank you girls for the moments and the amazing friendship.

I would like to thank Pedro Durão for the support, patience and crazy moments every day. Catarina Costa, Denise Camacho, Carmo Soares, Sara Júlio, Isaak, João Martins, Ana Queirós, Miguel Pinto, Patrícia Correia, Sara Mateus, Mariana Santos, Ana Cunha, Natacha Leonardo and Catarina Craveiro thank you for the relaxing times and for making me feel like home! You are amazing!

On a personal note, I want to express my profound gratitude to my family. I would like to thank my sister Sofia and my mother for always believing in me and my capabilities. I also would like to thank my dad for the encouragement, my baby sister Eva and my grandparents for having faith in me. Last, but not least I want to thank you my boyfriend, Gonçalo Andrade, for providing me unfailing support and encouragement. Thank you for never doubting that I would be able to conclude this journey.

Finally, I want to thank my friends: Rita Mateus, Rita Caneco, Fábio Vieira, Fábio Coelho, Bruno Rosa, Henrique Duarte, Patrícia Valentim, Catarina Abreu and Andreia Duarte. Without you it would definitely not be the same.

“Once you stop learning, you start dying”

Albert Einstein

Resumo

Um dos objetivos centrais da Neurociência é entender como é que o cérebro processa estímulos sensoriais e gera respostas comportamentais. Para atingir este objetivo é crucial monitorizar e manipular a atividade neuronal em tempo real, bem como estudar os circuitos neuronais e as suas conexões ao longo de todo o cérebro. Para facilitar esta tarefa é importante usar um organismo modelo geneticamente manipulável e com um sistema nervoso relativamente simples, mas com comportamento robusto. O peixe-zebra tem-se tornado um promissor organismo modelo no estudo do sistema nervoso. A acessibilidade e a transparência ótica dos embriões e larvas tornam possível a expressão e a visualização de repórteres fluorescentes geneticamente codificados, através de técnicas transgénicas. Neste trabalho foi usado um conjunto recente de repórteres fluorescentes geneticamente codificados (LSSmOrange, mScarlet e GCaMP6fEF05) para estabelecer novas linhas transgénicas, através do sistema de transposão *Tol2.* Estas linhas serão usadas para estudar a comunicação entre diferentes populações de neurónios e registar a atividade neuronal durante respostas comportamentais. A geração de novas ferramentas genéticas aliadas ao desenvolvimento de técnicas sofisticadas de imagem tem aberto a possibilidade de mapear todo o cérebro do peixe-zebra com elevada resolução e precisão temporal. Nos próximos anos, o desafio será combinar as metodologias desenvolvidas e correntemente usadas em peixe-zebra para entender os comportamentos gerados em vertebrados mais complexos.

Palavras-Chave: peixe-zebra; LSSmOrange; mScarlet; indicadores de cálcio geneticamente codificados; circuitos neuronais; neurobiologia.

Abstract

A central goal of Neuroscience is to understand how the brain processes sensory stimuli and generates behavioral responses. To achieve this goal, it is crucial to monitor and manipulate the neuronal activity of single cells in real time, as well as to study the neuronal circuits and their connections throughout the whole-brain in a behaving animal. Thus, it is important to use a genetically tractable model organism with a relatively simple nervous system but with robust behavior. Zebrafish has become a promising model organism in the study of nervous system. The accessibility and optical transparency of embryos and larvae make possible the expression and visualization of genetically encoded fluorescent reporters, through transgenic techniques. In this work, recent genetically encoded fluorescent reporters (LSSmOrange, mScarlet and GCaMP6fEF05) were used for establishing new transgenic zebrafish lines, through the *Tol2* transposon system. These lines will be used to study the communication between different populations of neurons and to record neural activity during behavioral responses. The generation of new genetic tools allied to the development of sophisticated imaging techniques has opened up the possibility of whole-brain imaging with single-cell resolution and high temporal precision. In the coming years, the challenge will be to combine the approaches developed and currently used in zebrafish to understand how behaviors are generated in higher vertebrates.

Keywords: zebrafish; LSSmOrange; mScarlet; genetically encoded calcium ion indicators; neuronal circuits; neurobiology.

Contents

Index of Figures

Index of Tables

Abbreviations

BFP - blue fluorescent protein

bp - base pairs

CaM - calmodulin

cDNA - complementary DNA

CFP - cyan fluorescent protein

CRISPR - clustered regularly interspaced short palindromic repeats

DiI - 1,1′-Dioctadecyl-3,3,3′,3′-tetramethylindocarbocyanine perchlorate

DiO - 3,3′-Dioctadecyloxacarbocyanine perchlorate

DNA - deoxyribonucleic acid

dpf - days post fertilization

E.coli - *Escherichia coli*

E3 - embryo medium

FRET - fluorescence resonance energy transfer

GECI - genetically encoded calcium ion indicators

GFP - green fluorescent protein

H2B - histone 2B

hpf - hours post fertilization

Isl3 - islet3

kb - kilobases

kz - Kozak sequence

LB - Luria-Bertani

mRFP - monomeric red fluorescent protein

mRNA - messenger RNA

ng - nanograms

OKR - optokinetic response

OMR - optomotor response

PBS - phosphate-buffered saline

PCR - polymerase chain reaction

PFA - paraformaldehyde

RFP - red fluorescent protein

RGC - retinal ganglion cells

rSyp - rat synaptophysin

Ta - annealing temperature

TAE - tris-acetate-EDTA

TALENs - transcription activator-like effector nuclease

TE - tris-EDTA

Tg - transgenic

TILLING - transcription activator-like effector nuclease

Tm - melting temperature

Tricaine - 3-amino benzoic acidethylester

TU - Tuebingen

UAS - upstream activating sequence

YFP - yellow fluorescent protein

I. Introduction

1. The challenge of Neuroscience

The central goal of Neuroscience is understanding how neuronal networks process sensory information in the brain and generate appropriate behaviors. However, this goal is particularly challenging, since it requires an understanding of neuronal networks from the biophysical properties of neurons to their interactions (Feierstein *et al.* 2015; Friedrich *et al.* 2013; Orger 2016). To accomplish this goal, it is essential to use a multidisciplinary approach involving several scientific fields, such as: genetics, molecular biology, optics, neurobiology and mathematical modelling, and the study of a model organism with a relatively simple nervous system but with robust behavior. Zebrafish is a promising model organism to address this challenge, as it allows to visualize and manipulate activity in neuronal circuits throughout the brain (Sumbre & de Polavieja 2014).

2. Zebrafish as a model organism

Zebrafish*, Danio rerio,* is a small shoaling tropical water fish native to rivers of south Asia, which belongs to *teleostei* infraclass (Orger 2016; Sumbre & de Polavieja 2014). Traditionally, zebrafish is used as model organism in genetic studies of embryonic development and organogenesis (Langheinrich 2003). However, it has become a popular model organism in biomedical research and neuroscience (Kalueff *et al.* 2014; Stewart *et al.* 2014). Although phylogenetically distant from humans, zebrafish has a nervous system organized like all vertebrates and shares a high genetic similarity to humans. Its genome has approximately 70% of homology with the human genome (Figure I.1) (Stewart *et al.* 2014) and 82% of orthologous human disease-related genes (Gutiérrez-Lovera *et al*. 2017; Santoriello & Zon 2012).

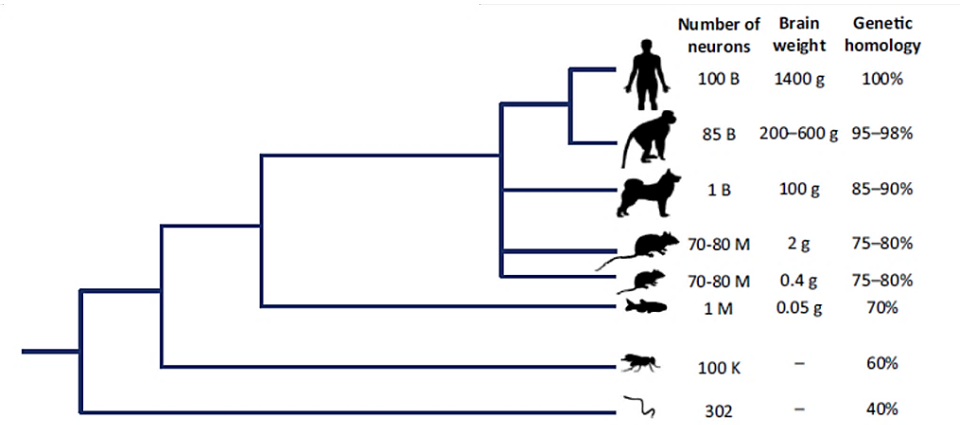

Figure I.1 – Phylogenetic tree of major model species. Adapted from Stewart *et al.* 2014.

Comparing with other *in vivo* models, zebrafish offers many advantages. Zebrafish has high fecundity and produces 200-300 embryos per mating pair and week. The embryos develop outside the mother's body and are transparent during the development stage, which enables a

non-invasive assessment of their internal structures, morphogenetic tissue movements, organogenesis, cellular interaction and subcellular dynamics in real time (Giannaccini *et al.* 2014; Gutiérrez-Lovera *et al.* 2017; Santoriello & Zon 2012). Furthermore, the optical clarity of zebrafish embryos is also an advantage for *in vivo* neuronal network analysis and neuronal activity monitoring (Stewart *et al.* 2014).

Zebrafish as a powerful model organism is also very cost-efficient, easy to raise and maintain and can be housed in large numbers in a minimal facility space (Ablain & Zon 2014; Kalueff *et al.* 2014). Moreover, it exhibits a very rapid embryonic development and a short generation time (two to three months). The major organs systems are formed 24 hours post fertilization (hpf) and the first behavioral responses appear at 3 days post fertilization (dpf). At 5 dpf, the larvae are able to swim, hunt for food, avoid predators and stabilize their position in moving water, which proves the existence of well-developed neuronal circuits (Feierstein *et al.* 2015; Giannaccini *et al.* 2014; Gutiérrez-Lovera *et al.* 2017; Renninger *et al.* 2011; Santoriello & Zon 2012).

Another strength of this model organism is that it is genetically tractable. The genetic approaches validated and currently used include generation of random mutations and subsequent gene or enhancer-trap screens (Patton & Zon 2011), morpholino knock-down (Bill *et al.* 2009; Lan *et al.* 2011), transcription activator-like effector nuclease (TALENs) system (Cermak *et al.* 2011; Joung & Sander 2012), targeting induced local lesions in genomes (TILLING) system (Moens *et al.* 2008), clustered regularly interspaced short palindromic repeats (CRISPR) technology (Chang *et al.* 2013; Hwang *et al.* 2013) and transgenesis using the *Tol2* transposon system (Kikuta & Kawakami 2009). The use of all these genetic approaches has allowed the generation of several transgenic and mutant zebrafish lines, which are particularly important in identifying human neural diseases (Stewart *et al.* 2014) and studying the development and function of the nervous system (Higashijima 2008; Sumbre & de Polavieja 2014).

3. Neuronal circuits underlying behaviors

In order to determine the organization and function of neuronal circuits underlying behavioral responses, sophisticated imaging techniques have been developed. These techniques have opened up the possibility to identify and label specific neurons, as well as to monitor and manipulate neuronal activity of single cells and entire circuits with high resolution (Friedrich *et al.* 2013; Renninger & Orger 2013; Sumbre & de Polavieja 2014). The combination of these imaging techniques, optogenetic tools and the larvae's small size and transparent skin enables the imaging of the whole-brain neuronal activity in larvae completely or partially restrained in low-melting agarose. When partially restrained, the eyes and tail are free to move, allowing the correlation between the neuronal activity to the behavioral responses (Renninger & Orger 2013; Sumbre & de Polavieja 2014).

One of the most studied behaviors is zebrafish is the visuomotor behavior (Portugues & Engert 2009). In early stages, vision is crucial for survival, since it allows larvae to hunt for food, avoid predators and navigate. Therefore, this strong evolutionary pressure leads to a rapid development of the visual system and a repertoire of visuomotor behaviors: startle response, optomotor response (Figure I.2A), optokinetic response (Figure I.2B) and prey capture. These behaviors can be elicited through visual stimuli in an artificial environment with larvae swimming freely or larvae partially restrained in low-melting agarose (Fleisch & Neuhauss 2006; Orger 2016; Renninger *et al.* 2011; Sumbre & de Polavieja 2014).

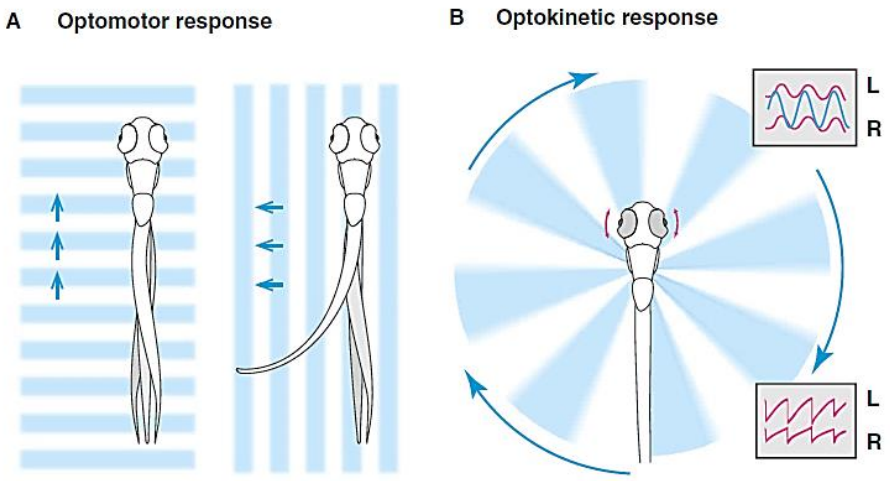

Figure I.2 – Visuomotor behaviors: optomotor response (A) and optokinetic response (B). (A) The optomotor response (OMR) is the ability of the larva to swim in the direction of a perceived motion evoked by a translational whole-field motion. The OMR divides in orienting turns, which serve to bring motion into a tail to head direction (right), and forward swims when the fish position is according to motion (left). **(B)** The optokinetic response (OKR) is a reflexive eye movement evoked by a whole-field rotational motion. During a rotational motion, fish adjust the direction of their eyes, alternating between slow eye movements to rapid saccades (pink traces, bottom box). Sinusoidal rotating stimulus (pink arrows) results in a consistent slow tracking movement (top box). The direction of motion is indicated by blue arrows. Adapted from Orger 2016.

Thus, to understand how neuronal circuits generate robust and complex behaviors, it is crucial to identify and characterize the neuronal populations involved in specific circuits and to delineate different areas involved in sensory processing and motor generation (Feierstein *et al.* 2015; Orger 2016). Moreover, it is also important to develop neuronal activity maps and put that activity in a context of neuroanatomy.

In the last years, a Z-Brain atlas, an open-source atlas that contains molecular labels and definitions of anatomical regions, was built. Using the Z-Brain atlas as a reference brain, it is possible to perform direct comparisons between experiments, describe regions of activity directly and reveal brain-wide functional connectivity patterns. These analyses become even more powerful as more labels and activity maps are accumulated in the Z-brain (Randlett *et al.* 2015). In order to increase the molecular labels and target specificity of identified cell types, several transgenic zebrafish lines have been generated (Renninger *et al.* 2011).

4. Transgenesis

Transgenesis is a powerful methodology for studying the function of genes and genomes in model plants and animals, and consisting of the introduction of an engineered DNA fragment into the genome of an organism (Kikuta & Kawakami 2009; Mosimann & Zon 2011). In zebrafish, the transgenesis is mainly achieved by integration of the gene of interest in its genome, through plasmid DNA microinjection in one-cell stage embryos. Traditionally, the non-*Tol2*-DNA microinjection method (Stuart *et al.* 1998) and the *I-SceI*-mediated method (Thermes *et al.* 2002) were used, but their limitations led to the development of other methodologies with high transgene integration efficiency. These methodologies include the *Sleeping Beauty* transposon system (Ivics *et al.* 1997) and *Tol2* transposon system (Kawakami *et al.* 2004). Taking advantage of the *Tol2* transposon system, the Gal4-UAS transactivation system, which will be explained later on, has been widely used to generate a large number of transgenic zebrafish lines.

4.1. *Tol2* transposon system

The *Tol2* transposable element was identified from the genome of the Japanese medaka fish (*Oryzias latipes*) and belongs to the *hAT* family of transposons (Koga *et al.* 1996). Although the vertebrate genome contains a large number of transposons, the *Tol2* element is the only autonomous transposable element identified in a vertebrate genome (Kawakami *et al*. 2000; Urasaki *et al.* 2006).

The *Tol2* transposable element is about of 4.7 kilobases (kb) in length and encodes a fully functional transposase protein capable of catalyzing transposition (Kawakami *et al*. 1998; Kawakami & Shima 1999). For that, the presence of minimal *Tol2 cis-sequences (Tol2* arms), that are recognized by the transposase (Figure I.3), is necessary. Theoretically, any DNA fragment can be cloned between *Tol2 cis-sequences.* It has been described that a *Tol2* construct can carry 11 kb DNA without reducing the transposition activity (Kawakami 2007; Urasaki *et al.* 2006).

Figure I.3 – Structure of the *Tol2* transposable element. *Tol2* transposable element encodes a mRNA for the transposase protein. Lines and dotted lines indicate the exons and introns, respectively. Black boxes represent coding regions and grey boxes represent untranslated regions. The terminals (L and R) correspond to the minimal *Tol2 cis-sequences* necessary for transposition. The minimal *Tol2 cis-sequences* are DNA sequences with 200 base pairs (bp) from the left end (L) and 150 bp from the right end (R) of the *Tol2* transposable element. Adapted from Kawakami 2007.

To facilitate transgenic studies in zebrafish, transgenic methods using the *Tol2* transposable element have been developed. The most popular approach is the *Tol2* transposon system. It

consists of two components: plasmid DNA carrying a non-autonomous *Tol2* construct and transposase mRNA synthesized *in vitro* by using the transposase cDNA as a template.

In zebrafish, stable transposition is achieved when a plasmid DNA and the transposase mRNA are co-injected into one-cell stage zebrafish embryos. The transposase protein is translated from the mRNA and catalyzes the excision of the non-autonomous *Tol2* construct from the plasmid, which is randomly integrated into the genome during early stages of embryonic development. Some *Tol2* constructs will be integrated in germ cells and transmitted to the offspring (Figure I.4). When the mRNA and transposase protein are degraded, the transposase activity ends, and the insertions become stable (Abe *et al.* 2011; Kawakami 2004; Kawakami 2007). The *Tol2* constructs are integrated in the genome through the cut-and-paste mechanism and the only modification observed is an 8 bp duplication at the integration site (Kawakami 2007; Kawakami *et al.* 2000).

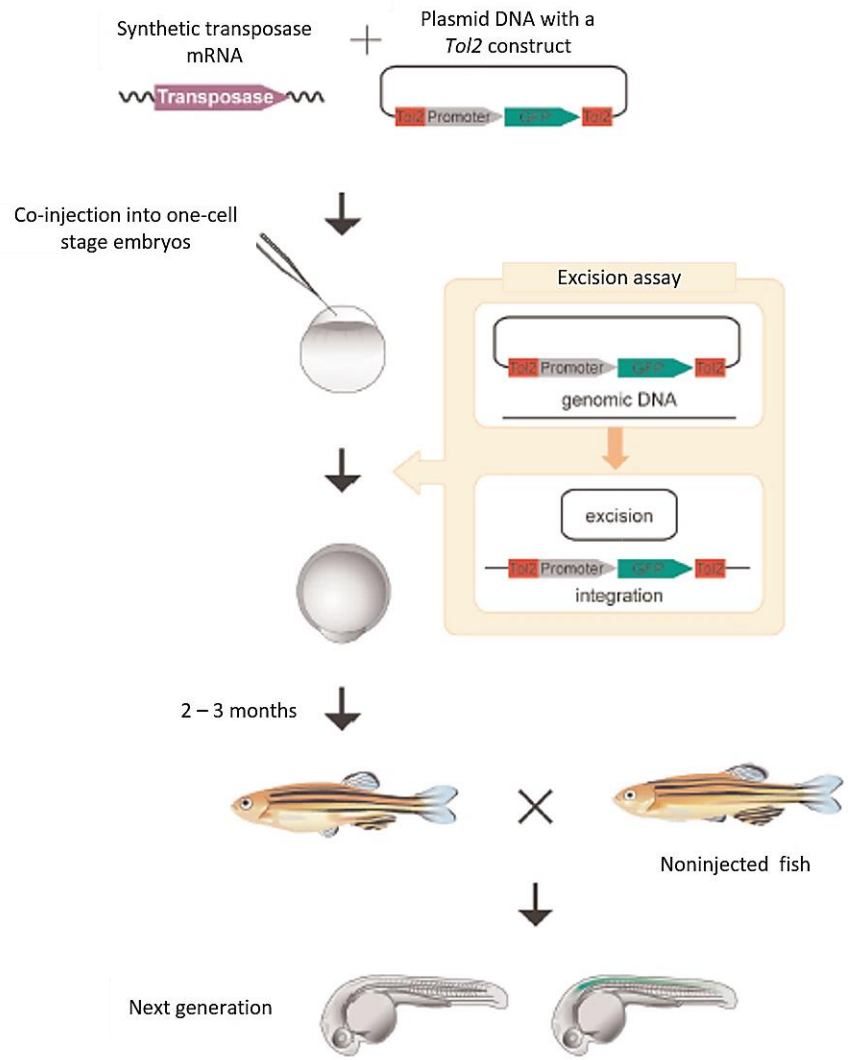

Figure I.4 – Scheme of transposition of a *Tol2* construct in zebrafish. The synthetic transposase mRNA and a plasmid DNA containing a *Tol2* construct are co-injected into one-cell stage zebrafish embryos. The *Tol2* construct is excised from the plasmid DNA and integrated into the zebrafish genome. The injected embryos are raised into adulthood and posteriorly mated with noninjected fish. The integrated *Tol2* constructs in germ cells are transmitted to the next generation. Adapted from Kawakami 2007.

4.2. Gal4-UAS transactivation system

Although the Gal4-UAS transactivation system has been extensively used in genetic studies in *Drosophila melanogaster*, it was not applied to genetic studies in vertebrates for a long period of time, mainly due to the lack of an efficient transposon system. However, this situation was revolutionized when the *Tol2* transposon system was developed in zebrafish (Asakawa & Kawakami 2008).

The Gal4-UAS transactivation system is a powerful genetic method that includes two components: the Gal4 protein and an Upstream Activating Sequence (UAS). The Gal4 protein is a yeast transcriptional activator that contains two domains: the DNA-binding domain and the transcription activation domain. The Gal4 protein binds to specific sites of the upstream activating sequence and activates the transcription of a target gene (Figure I.5) through the transcription activation domain (Asakawa & Kawakami 2008; Giniger & Ptashne 1987; Keegan *et al.* 1986; Ma & Ptashne 1987), which recruits the general transcriptional machinery to the promoter region (Traven *et al.* 2006).

To induce a strong expression of a target gene, the Gal4 protein can be modified. The Gal4-VP16 protein contains the DNA-binding domain from Gal4 and the transcriptional activation domain from the herpes simplex virus VP16 protein (Asakawa & Kawakami 2008; Sadowski *et al.* 1988). The Gal4FF (or GFF) protein contains the DNA-binding domain from Gal4 and two short transcriptional activation motifs from VP16 (Asakawa & Kawakami 2008; Seipel *et al.* 1992). Although Gal4FF shows a weaker transcriptional activity than Gal4-VP16, it is better tolerated in vertebrate cells, since high levels of expression of Gal4-VP16 inhibit the transcription of the target gene (Asakawa & Kawakami 2008).

The Gal4-UAS transactivation system is based on two types of transgenic lines: driver lines and reporter lines. While in driver lines the gene encoding Gal4 protein is placed under the control of a specific promotor; in reporter lines the gene of interest (*e.g.* genetically encoded fluorescent reporter gene) is linked to the UAS. This enables any gene of interest placed downstream of the UAS can be ectopically expressed in cells where the *gal4* gene is express. The expression of the gene of interest will reflect the expression pattern of Gal4, which is controlled by a promoter (Figure I.5) (Halpern *et al.* 2008; Scheer & Campos-Ortega 1999; Scott 2009). Promoters, such as *elavl3* (HuC) (Higashijima *et al.* 2003) and *alpha-1-Tubulin* (Hieber *et al.* 1998) are usually used to drive expression to most neurons throughout the nervous system (pan-neuronal expression pattern). Other promotors, such as *islet3* (*isl3*) and *ath5,* are commonly used to drive expression to specific regions. The Isl3 expression pattern is characterized by expression in retinal ganglion cells (RGCs), hindbrain, trigeminal nerve, spinal cord and optic tectum (Thisse & Thisse 2004; Renninger & Orger 2013). The Ath5 expression pattern is characterized by expression in RGCs (Renninger & Orger 2013).

The binary nature of the Gal4-UAS transactivation system enables the creation of several driver and reporter lines that can be combined in different ways, in order to generate a large number of transgenic zebrafish lines. These transgenic lines can be used to study the anatomy and connectivity of the nervous system and to identify neuronal circuits that regulate specific behavioral responses (Halpern *et al.* 2008; Scheer & Campos-Ortega 1999; Scott 2009).

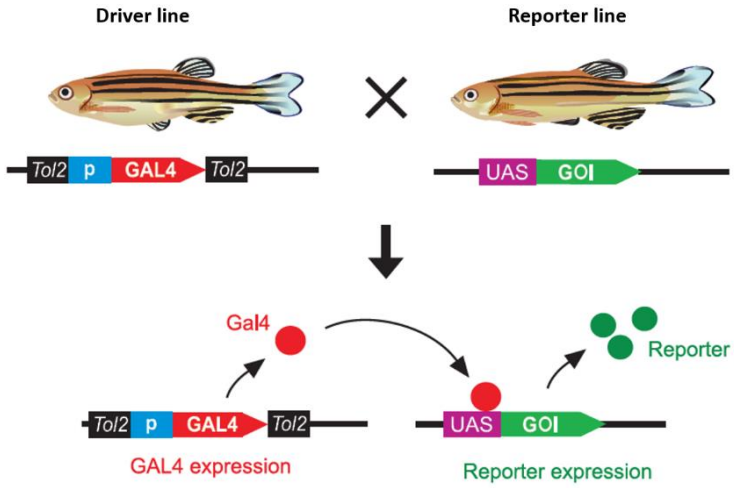

Figure I.5 – Gal4-UAS transactivation system in zebrafish. When a driver line with a specific promoter upstream of the *gal4* gene is crossed with a reporter line that carries a gene of interest (GOI) under the control of the UAS, the result is a double transgenic progeny. The gene of interest is expressed in Gal4-expressing cells. Adapted from Asakawa & Kawakami 2008.

5. Genetically encoded fluorescent reporters and subcellular localization tags

Transgenic techniques and optical transparency of zebrafish embryos and larvae make the zebrafish an ideal organism for studying neuronal connectivity, tracking neurons and monitoring neuronal activity in real time, through genetically encoded fluorescent reporters (Halpern *et al.* 2008; Renninger *et al.* 2011). After the discovery of green fluorescent protein (GFP) (Prasher *et al.* 1992), multiple genetically encoded fluorescent reporters have been developed to expand the color palette and improve the fluorophores characteristics, such as: folding speed, brightness, maturation, photostability, sensitivity and Stokes shift, *i.e.* the spectral distance between absorption and emission peaks of a fluorophore (Chudakov *et al.* 2010; Weber & Koster 2013). Furthermore, in order to visualize and study specific events, genetically encoded fluorescent reporters can be fused to subcellular localization tags (Weber & Koster 2013).

5.1. Genetically encoded calcium ion indicators

Genetically encoded calcium ion indicators (GECIs) are powerful approaches for monitoring the neuronal activity *in vivo*. GECIs not only allow the labeling of single neurons and neuronal populations, but they also have a long-term expression (Akerboom *et al.* 2013; Ni *et al*. 2017).

Neuronal activity can be recorded by changes in intracellular calcium concentration. Calcium ions (Ca^{2+}) are transported into neurons during action potential firing and synaptic input and, therefore, changes in intracellular calcium concentration are a good readout of ongoing neuronal activity (Akerboom *et al*. 2012; Akerboom *et al.* 2013; Ni *et al*. 2017; Renninger & Orger 2013).

The most optimized GECIs are single-wavelength green indicators based on the original genetically encoded calcium sensor, GCaMP. In the GCaMP sensor, GFP is fused to Calmodulin (CaM) and M13 peptide from the myosin light chain kinase. When Ca^{2+} is present, calmodulin binds to the M13 peptide, producing a conformational change in CaM-M13 interaction, which causes an increase of fluorescence intensity. GCaMP exhibits an excitation and emission maxima of ~484 nm and ~507 nm, respectively (Figure I.6) (Chudakov *et al.* 2005; Nagai *et al.* 2001; Ni *et al*. 2017; Renninger & Orger 2013).

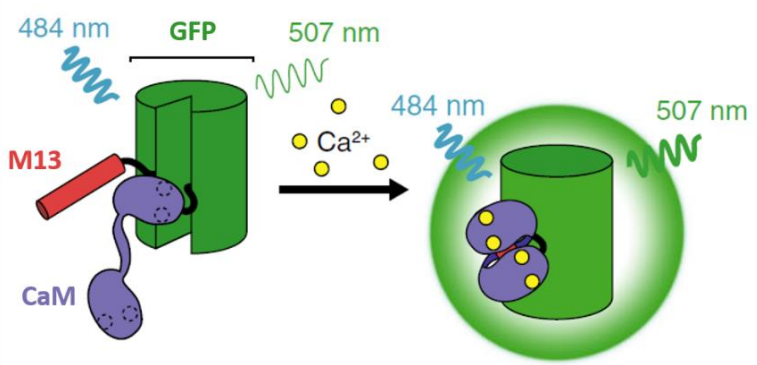

Figure I.6 – Genetically encoded calcium ion indicator GCaMP. In the presence of Ca^{2+}, calmodulin (CaM) binds to the M13 peptide, causing a conformational change in CaM-M13 interaction, which leads to an increase of brightness. Adapted from Ni *et al*. 2017.

The high levels of fluorescence and the high sensitivity of GCaMPs, in terms of signal-to-noise ratio and kinetics response, are the most important parameters to a successful detection of neuronal activity. The first version of GCaMP was not sensitive enough to reliably detect the fast calcium dynamics associated with neuronal activity *in vivo*, thus a high number of GCaMP variants have been produced, in order to increase its brightness and sensitivity. The GCaMPs that exhibit the best performance belong to the GCaMP6 family (Chen *et al.* 2013; Ni *et al*. 2017; Renninger & Orger 2013). This family is able to detect single action potential and includes three ultrasensitive GCaMP6 sensors: GCaMP6s, GCaMP6m and GCaMP6f, that show slow, medium and fast kinetics, respectively (Chen *et al.* 2013).

Recently, new variants of GCaMP6s and GCaMP6f have been developed by Michael Orger's Laboratory (Champalimaud Centre for the Unknown), through an extensive mutagenesis study. Visually evoked activity was characterized under the two-photon microscope for the different GCaMP mutation combinations in zebrafish larvae and mouse hippocampal slice cultures. This study offered several GCaMP6 variants to select from, with overall brightness, rise/decay kinetics and calcium affinity tuned for diverse applications (Tomás *et al.* unpublished data).

Another favorable feature of GCaMPs is the possibility to modulate the color of the fluorescent protein. Direct mutations in the GFP chromophore result in fluorescent proteins with different excitation/emission properties (BFP, CFP, YFP, RFP – blue, cyan, yellow, red fluorescent proteins). These proteins can be fused with biosensors to obtain GECIs. For imaging, red-shifted indicators are preferable, since longer wavelengths reduce the tissue scattering, autofluorescence and phototoxicity. Moreover, non-green sensors offer the possibility to use animals that express GFP (Akerboom *et al.* 2013).

5.2. LSSmOrange

Multicolor imaging based on genetically encoded fluorescent proteins is a powerful tool to study dynamic processes in living cells. One of the most recently developed genetically encoded fluorescent proteins is LSSmOrange (Shcherbakova *et al*. 2012).

LSSmOrange is a monomeric orange fluorescent protein (mOrange) with a large energy gap between the excitation and emission peaks, currently designed by Light-induced Spectral Shift (LSS) (Fron *et al.* 2015). LSSmOrange exhibits an excitation and emission maxima of 437 nm and 572 nm, respectively (Figure I.7), and a highest brightness than red LSS fluorescent proteins (Shcherbakova *et al*. 2012). Moreover, it also exhibits a photoconvertible process, which can be characterized by a shift of the excitation maximum from 437 to 553 nm without changing the emission spectrum (Bergeler *et al.* 2016; Fron *et al.* 2015).

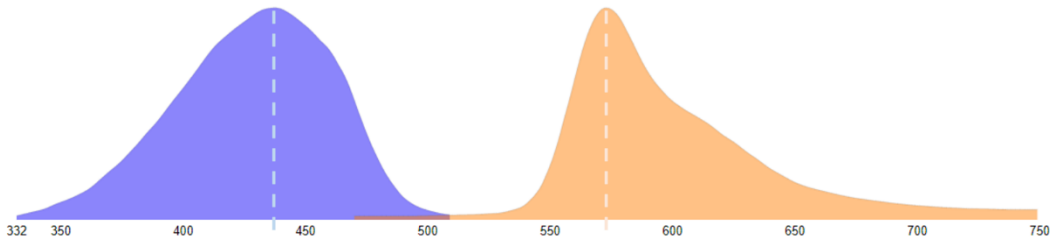

Figure I.7 – LSSmOrange fluorescence absorbance (blue) and emission (orange) spectra. LSSmOrange has an excitation maximum of 437 nm and an emission maximum of 572 nm. Adapted from FPbase (https://www.fpbase.org/, consulted on 29/08/2018).

The well-separated absorption and emission spectra, typically more than 100 nm, is a great advantage in multicolor fluorescence microscopy with a single laser wavelength, since a laser can simultaneously excite various fluorescent proteins with similar excitation, but different emission maxima (Chudakov *et al.* 2010; Fron *et al.* 2015; Keersmaecker *et al.* 2015). In addition, LSSmOrange using a single-wavelength excitation also enable other multicolor applications in flow cytometry and fluorescence resonance energy transfer (FRET) (Shcherbakova *et al*. 2012).

5.3. mScarlet

The wide expansion of the fluorescent proteins occurred after discovery of red fluorescent proteins (RFPs). RPFs usually form tetramers, which interfere with function and localization of the RPF-fusion proteins. In order to solve this limitation, various monomeric proteins have been created, but the monomerization leads to a significant deterioration of brightness. One of the main goals of fluorescent protein engineering has been to develop bright monomeric fluorescent reporters with a complete maturation (Bindels *et al*. 2017; Rodriguez et al. 2017). mScarlet is the latest brighter monomeric red fluorescent protein developed (Bindels *et al*. 2017).

mScarlet was generated from a synthetic template through improved screening techniques, and it exhibits an excitation and emission maxima of 569 nm and 594 nm, respectively (Figure I.8). Comparing with other RPFs, mScarlet offers many features that make it a powerful monomeric RFP (mRFPs). mScarlet shows the highest fluorescence lifetime (3.9 ns) and the highest quantum yield (0.7) recorded in the mRFPs and exhibits a record brightness ($71x10^3$ $M^{-1}cm^{-1}$) in the mRFP spectral class. Moreover, mScarlet shows a complete maturation and a high tolerance in acidic environments, since it has a low pK_a (5.3) (Bindels *et al*. 2017).

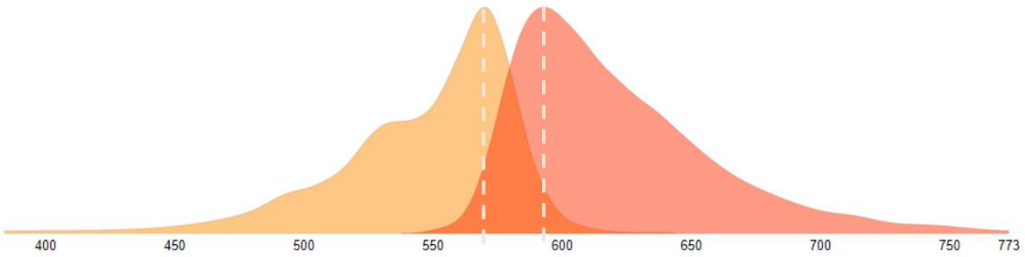

Figure I.8 – mScarlet fluorescence absorbance (orange) and emission (red) spectra. mScarlet has an excitation maximum of 569 nm and an emission maximum of 594 nm. Adapted from FPbase (https://www.fpbase.org/, consulted on 29/08/2018).

The creation of mScarlet led to the development of two variants with a single amino acid substitution: mScarlet-I and mScarlet-H. Although these variants exhibit a lower fluorescence lifetime and quantum yield than mScarlet, mScarlet-I has an enhanced maturation and mScarlet-H has an improved photostability. None of mScarlets shows problems of cytotoxicity, photochromicity, dimerization or incomplete maturation. Furthermore, mScarlet and their variants are the preferred monomeric RFPs for cellular microscopy and quantitative functional imaging, since they can be used as an RPF fusion tag for labeling various subcellular structures and organelles in live cells, or as a FRET acceptor in radiometric imaging (Bindels *et al*. 2017).

5.4. Subcellular localization tags

In order to visualize and study specific events, genetically encoded fluorescent reporters can be fused to subcellular localization tags, which allows to restrict the fluorescent reporter expression to a specific subcellular localization or structure (Weber & Koster 2013).

In zebrafish, the histone 2B sequence (H2B tag) is commonly used, since it directs the fluorescent reporter expression to the nucleus (Halpern *et al.* 2008; Weber & Koster 2013). Another example is the rat synaptophysin sequence (rSyp tag), that directs the fluorescent reporter expression to presynaptic vesicles (Meyer & Smith 2006). Thus, any cellular compartments and structure can be highlighted as long as there is a specific protein to direct the fluorescent reporter expression to those compartments and structures.

6. Aims

The central aim of this project is to generate new transgenic zebrafish expressing recent genetically encoded fluorescent reporters, as these fluorescent reporters offer unique advantages in fluorescence microscopy imaging of the whole-brain neuronal activity, quantitative analysis of behavior and study of neuronal circuits underlying visuomotor behaviors.

The specific aims of this project are:

- To clone new genetically encoded fluorescent reporter genes (*LSSmOrange* and *mScarlet)*, into zebrafish expression vectors;
- To generate stable transgenic zebrafish lines by injecting expression clones into one-cell stage zebrafish embryos, using the *Tol2* transposon system;
- To characterize the fluorescent reporter expression in the new transgenic lines, using confocal microscopy.

II. Material and Methods

1. Molecular cloning

1.1. Expanding plasmid DNA from Addgene

Plasmids encoding the fluorescent reporter genes (*LSSmOrange* and *mScarlet*) were obtained from Addgene (https://www.addgene.org/) (Table II.1), and further cloned into a *Tol2* Gateway destination vector (Supplement A.1), constructed by Michael Orger's Laboratory (Champalimaud Centre for the Unknown).

Table II.1 – Original plasmids with genetically encoded fluorescent reporter genes, antibiotic resistance and bacteria growth temperature.

Fluorescent reporter gene	Original Plasmid	Antibiotic Resistance	Bacteria growth temperature (°C)
LSSmOrange	pH2B-LSSmOrange [(a)]	Kanamycin	37
mScarlet	pmScarlet_C1 [(b)]	Kanamycin	37

[(a)] pH2B-LSSmOrange was a gift from Vladislav Verkhusha (Addgene plasmid #37133). Map in supplement A.2A.
[(b)] pmScarlet_C1 was a gift from Dorus Gadella (Addgene plasmid #85042). Map in supplement A.2B.

In order to isolate a single colony, bacterial cultures were spread on Luria-Bertani (LB) broth agar plates (composition in table II.6) supplemented with kanamycin 50 µg/ml (Sigma #060615) and incubated overnight at 37°C.

1.2. Plasmid DNA isolation

Single colonies were inoculated into 4 ml of LB broth (composition in table II.6) supplemented with appropriate antibiotic and incubated overnight at 37°C with shaking. Plasmid DNA was obtained using the QIAprep Spin Miniprep Kit (QIAGEN #27106), according to the manufacturer's instructions. Unless otherwise specified, DNA was eluted in 5 mM of Tris HCl, pH 8.0. Antibiotics were used at the following concentrations: 100 µg/ml ampicillin (Sigma #A9518) and 50 µg/ml kanamycin (Sigma #060615).

Plasmid DNA was preserved in glycerol stocks. Under aseptic conditions, 800 µL of the bacterial culture were added to 800 µL of 100% (v/v) glycerol (Sigma #G2015). Glycerol stock tube was stored at - 80°C.

1.3. DNA quantification

DNA was quantified by ultraviolet spectrophotometry using a Nanodrop (ND-2000) spectrophotometer.

1.4. Polymerase Chain Reaction (PCR)

DNA fragments used in the cloning procedures were amplified by PCR. For each DNA fragment, sequence-specific primers were designed (Table II.2). PCR reactions were performed according to the recommended protocol for each DNA polymerase: Phusion High-Fidelity DNA Polymerase (NEB #M0530S) and Platinum SuperFi DNA Polymerase (Invitrogen #12351-010), using a C1000 Touch Thermal Cycler (BioRad).

For Phusion High-Fidelity DNA Polymerase, reaction mixes were prepared in volumes that ranged between 50 to 200 µL, depending on the application, using < 250 ng of template DNA, 10 mM of deoxynucleotide (dNTP) mix, 0.5 µM of each primer, 5X Phusion HF Buffer (1x) and 1U of Phusion DNA polymerase per 50 µL of reaction. DNA was amplified under the following thermocycling conditions: an initial melting step of 98°C for 3 minutes followed by 34 cycles of amplification, composed of denaturation at 98°C for 10 seconds, annealing at the appropriate temperature for 20 seconds and extension at 72°C for 30 seconds/kb. A final extension step was performed at 72°C for 10 minutes.

For the Platinum SuperFi DNA Polymerase, reaction mixes were prepared in volumes that ranged between 50 to 200 µL, depending on the application, using 100 ng of template DNA per 50 µL of reaction, 0.2 mM of dNTP mix, 0.5 µM of each primer, 5X SuperFi Buffer (1x) and 0.02 U/µL of Platinum SuperFi DNA Polymerase. DNA was amplified under the following thermocycling conditions: an initial melting step of 98°C for 30 seconds followed by 34 cycles of amplification, composed of denaturation at 98°C for 10 seconds, annealing at the appropriate temperature for 10 seconds and extension at 72°C for 30 seconds/kb. A final extension step was performed at 72°C for 5 minutes.

Table II.2 - Primers used for the amplification of DNA fragments, corresponding sequences and melting temperature (Tm).

Primer	Sequence	Tm (°C)
SpeI-**kz**-LSSmOrange_Fw	5'*CG*ACTAGT**GCCACCATGG**TGAGCAAGG 3' [(a)]	63.1
PacI-**Stop**-LSSmOrange_Rv	5'*GG*TTAATTAA**TTA**CTTGTACAGCTCGTCCATGCC 3' [(a)]	64.2
SpeI-**kz**-mScarlet_Fw	5'*GG*ACTAGT**GCCACCATGG**TG AGCAAGG 3' [(a)]	63.1
PacI-**Stop**-mScarlet_Rv	5'*CG*TTAATTAA**TTA**CTTGTACA GCTCGTCCATGCC 3' [(a)]	62.7
EcoRI-α1Tubpromoter_Fw	5'*CG*GAATTCCTGTAAGGTATATGAAAGCATTATTATTCTA AACATGTC 3'	70.8
α1TubuIntron1-LSSmOrange/mScarlet_Rv	5'GCCCTTGCTCACCTGTGAAGAAAAAGGCAAAAGTTAAA AGTCAAAC 3' [(b)]	70.4
α1Tubpromoter-(No ATG)-LSSmOrange_Fw	5'GCCTTTTTCTTCACAGGTGAGCAAGGGCGAGGAGAAT AAC 3' [(b)]	69.9
α1Tubpromoter-(No ATG)-mScarlet_Fw	5'GCCTTTTTCTTCACAGGTGAGCAAGGGCGAGGCAG 3' [(b)]	71.0

[(a)] Restriction sites are underlined in primers' sequence. Kozak sequence (kz) and stop sequence are in bold. Extra nucleotides to ensure the cleavage by restriction endonucleases are in italic.

[(b)] Overlap sequences for Gibson Assembly are in blue.

1.5. Agarose gel electrophoresis

PCR products or DNA fragments were separated according to size and visualized on agarose gels stained with GreenSafe Premium (nzytech #18011), according to the manufacturer's instructions. Gels were prepared using 1% (w/v) agarose (Fisher BioReagents #BP160-500) in 1x Tris-acetate-EDTA (TAE) (composition in table II.6) and the DNA samples were mixed with the Gel Loading Dye Purple (6x) (NEB #B7024S), prior to loading on wells. Fragment size was estimated by comparison with linear DNA standards of known molecular weight (GeneRuler 1 Kb DNA ladder, Thermo Scientific #SM0311, Supplement A.3). Electrophoresis was performed at 80-100V in 1x TAE buffer.

1.6. DNA extraction from agarose gel

DNA fragments were carefully excised from the gel and recovered with QIAquick Gel Extraction Kit (QIAGEN #28706), according to the manufacturer's instructions. Unless otherwise specified, DNA was eluted in 5 mM of Tris HCl, pH 8.0.

1.7. Restriction digestion

Restriction digestions of plasmids DNA or PCR products were prepared in a total volume of 20 µL, using the appropriate restriction endonucleases (NEB) and corresponding buffers (NEB) (Table II.3), according to the manufacturer's instructions. In the case of double digestion with different buffers, the buffer that provided the maximal activity for both enzymes was selected. Restriction digestions were incubated for 1 to 2 hours at 37°C.

Table II.3 – Restriction endonucleases used in restriction digestions and corresponding buffers.

Restriction endonuclease	Buffer
BstXI	NEBuffer 3.1
EcoRI-HF	CutSmart
HindIII	NEBuffer 2.1
NotI-HF	CutSmart
SacI-HF	CutSmart
SpeI-HF	CutSmart
PacI	CutSmart
PstI	NEBuffer 3.1

1.8. DNA purification

DNA fragments were purified with QIAquick PCR Purification Kit (QIAGEN #28106), according to the manufacturer's instructions. Unless otherwise specified, DNA was eluted in 5 mM of Tris HCl, pH 8.0.

1.9. DNA ligation

Digested DNA fragments (inserts) and vectors were ligated using T4 DNA ligase (NEB #M0202S). Approximately 50 ng of vector DNA was ligated with 3-fold excess of insert in a 20 µL reaction (made up in sterile Milli-Q water), containing 1x T4 ligase reaction buffer (NEB #B0202S) with 10 mM ATP (NEB #B0202S) and 1U of T4 DNA ligase. Ligation was performed from 30 minutes at room temperature to overnight at 4°C.

The amount of DNA insert (in ng) used in each reaction was calculated with the following formula:

$$\text{ng insert} = \frac{50 \text{ ng vector} \times \text{kb insert}}{\text{kb vector}} \times 3$$

1.10. Transformation of competent cells

Escherichia coli chemically competent cells were transformed by heat shock method, according to Froger & Hall 2007. All competent cells used were stored at - 80°C. The thawing process was performed on ice for 5 minutes. Then, the aliquots were incubated on ice for 30 minutes with 3 to 10 µL of ligation mix. The DNA-cells mix was then heat shocked for 30 seconds at 37°C, followed by 2 minutes on ice. Under aseptic conditions, 500 µL of LB medium were added to the mix and incubated for 1 hour at 37°C with shaking. Cells were plated on LB broth agar plates containing the appropriate antibiotic and incubated overnight at 37°C. Ampicillin was used at 100 µg/ml and kanamycin at 50 µg/ml. In this work, TOP10 chemically competent *E.coli* and *ccdB* Survival 2 competent cells were used, whenever appropriate.

1.11. DNA sequencing

Plasmid DNA integrity was confirmed by sequencing. DNA was sequenced at STAB VIDA according to the Sanger method, using specific or general primers (Table II.4). DNA sequences were analyzed and compared with the desired DNA sequences using SnapGene (sequence analysis software that allows for planning, visualization and documentation of molecular biology procedures) (http://www.snapgene.com/). Sequencing samples were prepared in a total volume of 10 µL (made up in sterile Milli-Q water), containing 100 ng of plasmid DNA and 3 µL at 10 µM of sequencing primer.

Table II.4 – Primers used for the DNA sequencing, corresponding sequence and melting temperature (Tm).

Primer	Sequence	Tm (°C)
SV40_Rv	5'ACTGCATTCTAGTTGTGGTTTGTCC 3'	63.0
M13_Fw	5'GTAAAACGACGGCCAGT 3'	56.3
M13_Rv	5'CAGGAAACAGCTATGAC 3'	50.7
α1Tub225_Fw	5'GTTGGGCCTGCTCCTCATTC 3'	62.7
α1Tub450_Fw	5'GATGCGACTGGATGTTGAGG 3'	60.1
α1Tub-intron87_Fw	5'GTAGTCACGGTTGTGCTTATAACC 3'	60.7
α1Tub271_Rv	5'GGAGATGAATAATGGTGTTGCTTGG 3'	61.6

1.12. Gateway cloning technology - LR recombination reaction

The LR recombination reaction was performed using the Gateway LR Clonase II Enzyme Mix Kit (Invitrogen #11791-020), according to the manufacturer's instructions. The reaction containing 150 ng of destination vector, 150 ng of entry clone and 2 µL of Gateway LR Clonase II Enzyme Mix was prepared in a total volume of 10 µL (made up in Tris-EDTA (TE) buffer, composition in table II.6) and incubated for 3 hours at 25°C. Then, 1 µL of Proteinase K was added and the LR reaction was incubated for 10 minutes at 37°C. The 10xUAS Entry Clone (Supplement A.4) was constructed by Michael Orger's Laboratory (Champalimaud Centre for the Unknown).

1.13. Gibson Assembly

Gibson Assembly was performed using the Gibson Assembly Master Mix Kit (NEB #E2611L), according to the manufacturer's instructions. The reaction containing 10 µL of 2x Gibson Assembly Master Mix was incubated with 2 fragments (0.5 pmol each) in a total volume of 20 µL for 1 hour at 50°C. The *alpha-1-Tubulin* fragment was obtained from a pT-alpha1Tubulin-GCaMP vector (Supplement A.5), constructed by Michael Orger's Laboratory (Champalimaud Centre for the Unknown). This fragment contains the promoter, first exon and first intron of the *alpha-1-Tubulin* gene.

1.14. Adding 3'-A overhangs

PCR product was incubated with 100mM of ATP (Thermo Scientific #R1441) and 1U of Taq Polymerase (NEB #M0273S) in Standard Buffer Taq Polymerase (1x) for 10 minutes at 72°C to add 3' deoxyadenosine (A) overhangs.

1.15. TA Cloning

PCR product was cloned into a pCR2.1-TOPO vector (Supplement A.6) using the TOPO TA Cloning Kit (Invitrogen #45-0641), according to the manufacturer's instructions. Then, 4 µL of PCR product with 3'-A overhangs was added to 1 µL of the pCR2.1-TOPO vector along with 1 µL of high salt solution. Ligation was performed from 30 minutes at room temperature to overnight at 4°C.

2. Transgenesis

2.1. Animal handling and welfare

All *in vivo* experiments were performed using zebrafish *(Danio rerio*) from the Fish Platform at the Champalimaud Centre for the Unknown. Zebrafish were handled according to European animal welfare regulations and standard protocols, following the Champalimaud Fish Platform program (Martins *et al.* 2016).

Adult zebrafish were maintained at 28ºC in a holding room with 14 hours light/10 hours dark cycle, using 200-300 lux ambient light intensity. They were kept in 3.5L tanks with running water and a maximum population of 10 fish per liter. Moreover, adult zebrafish were fed twice a day, in the morning they were fed living aquatic crustaceans *Artemia nauplii* and in the afternoon they were fed a nutritive dry powder, Zebrafeed 400-600 (sparos). Physical and chemical parameters of the fish water - temperature, pH, conductivity, dissolved gases, nitrates, nitrites and ammonia - were kept within physiological values (Martins *et al.* 2016).

2.2. Zebrafish strains

In this work, three different zebrafish strains were used: Tuebingen (TU), *nacre*$^{-/-}$ and Tg (Isl3:Gal4$^{+/+}$). TU is a popular wild-type strain. *nacre* $^{-/-}$ is a recessive mutant strain, where the homozygous mutants have a complete lack of melanophores throughout all life stages due to a single-base mutation in the *mi*crophthalmia-associated *t*ranscription *f*actor *a* (*mitfa)* gene, which is required for melanophores' development. Nevertheless, these fish have a normal development of the pigmented epithelium of the retina (Lister *et al.* 1999). Last, but not least, Tg (*Isl3:Gal4*$^{+/+}$) is a driver line that activates Gal4 expression under the control of the *Isl3* promoter. This Tg (*Isl3:Gal4*$^{+/+}$) line has a heart-specific GFP marker (Huang *et al.* 2003).

2.3. Microinjection in one-cell stage zebrafish embryos

Microinjection is a method used for generating transgenic fish through the introduction of genetic material into fertilized zebrafish embryos. Microinjection was performed into one-cell stage embryos, according to Kikuta & Kawakami 2009.

2.3.1. Crossing adult zebrafish

Zebrafish embryos used in the microinjection experiments were obtained by crossing adult zebrafish in breeding tanks. Breeding tanks have a grid that allows the eggs to fall and protects the embryos from being eaten by adults. The night prior to the microinjection, zebrafish were transferred into breeding tanks with a plastic barrier to separate males and females. The ratio used was three males to five females. In the following morning, the plastic barriers were removed to enable mating. Approximately 20 minutes after the mating time, fertilized eggs were harvested and transferred into petri dishes with 1x embryo medium (E3) (composition in table II.6). In the end, the zebrafish adults were transferred back to the fish facility's main system.

Isl3:Gal4$^{+/+}$ transgenic embryos were used in case of the UAS constructs (Table II.5) and *nacre*$^{+/-}$ embryos were used in case of the *alpha-1-Tubulin* construct (Table II.5). The *nacre*$^{+/-}$ embryos resulted from the crossing between TU and *nacre*$^{-/-}$ adult zebrafish.

Table II.5 – Zebrafish strains used for the microinjection of the expression vectors.

Expression vector	Zebrafish strain
pTol2-10xUAS:rSyp-mCherry [(a) (b)]	Tg (*Isl3:Gal4*$^{+/+}$)
pTol2-10xUAS:rSyp-GCaMP6fEF05 [(a) (c)]	Tg (*Isl3:Gal4*$^{+/+}$)
pTol2-10xUAS-mScarlet	Tg (*Isl3:Gal4*$^{+/+}$)
pTol2-alpha1Tubulin-mScarlet	*nacre* $^{+/-}$

(a) Expression vector constructed by Michael Orger's Laboratory (Champalimaud Centre for the Unknown).
(b) Map in supplement A.7A.
(c) Map in supplement A.7B.

2.3.2. Preparation of the injection mixture and needles

Prior to microinjection, an injection mixture with a total volume of 10 µL (made up in E3-Phenol Red, composition in table II.6), containing 18 ng/µL of expression vector (Table II.5) and 100 ng/µL of *Tol2* transposase mRNA, was prepared on ice. The injection mixture remained on ice until it was loaded into the microinjection needle. Microinjection needles were previously made from glass capillaries (World Precision Instruments Inc.), using a Laser-Based Micropipette Puller (Sutter Instrument P-2000) with the following settings: heat = 400, filament = 4, velocity = 45, delay = 200 and pull = 100.

2.3.3. Injection

Zebrafish embryos were aligned in the trenches of the injection plate (1% (w/v) agarose in 1x E3) (Figure II.1A) and the surplus water was removed. A needle was loaded with 3 µL of injection mixture and attached to the Pneumatic PicoPump PV 820 (World Precision Instruments Inc.). The tip of the needle was broken using forceps.

Under a stereoscope (Zeiss SteREO Discovery.V8), the injection mixture was microinjected into the cell of each zebrafish embryo (Figure II.B). When all embryos were injected, they were carefully harvested into a petri dish with 1x E3 and incubated at 28°C. In the following day, they were bleached, according to Martins *et al.* 2016 and raised in the fish facility's main holding room.

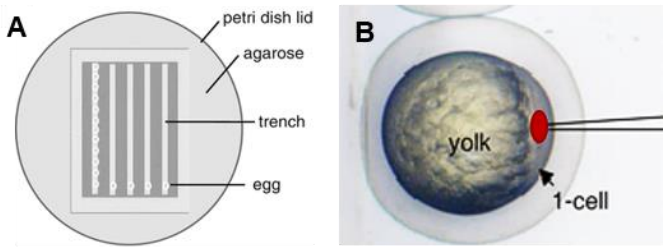

Figure II.1 – **Microinjection in one-cell stage zebrafish embryos. (A)** Schematic representation of an injection plate. Adapted from Wang *et al.* 2013. **(B)** Schematic representation of the microinjection in one-cell stage zebrafish embryo. The needle softly perforates the chorion until reaches the cell where the injection mixture (red spot) is microinjected, through a short air burst. Adapted from Zhang & Wiest 2016.

2.4. Screening for transient expression

Injected embryos were pre-screened for transient expression of the fluorescent reporter genes between 2-3 dpf, by fluorescence microscopy (Zeiss StrREO Discovery.V8 equipped with PentaFluar). Embryos injected with pTol2-10xUAS:rSyp-GCaMP6fEF05 were screen with a blue filter with a spectrum range from 400-460 nm. Embryos injected with pTol2-10xUAS:rSyp-mCherry, pTol2-10xUAS-mScarlet or pTol2-alpha1Tubulin-mScarlet were screened with a green filter with a spectrum range from 545-606 nm.

Based on fluorescence intensity and expression patterns, positive injected embryos were selected to be raised into adulthood. Embryos were selected for the Isl3 (*isl3* promoter) and pan-neuronal (*alpha-1-Tubulin* promoter) expression pattern.

2.5. Screening for stable expression

When the positive injected fish (generation F-1) reached sexual maturity (two to three months), a cross with the same zebrafish strains used for the microinjection was performed. The progeny was screened for stable expression, between 2-3 dpf, by fluorescence microscopy. Positive embryos (F0 generation or founders) were selected to be raised into adulthood, based on fluorescence intensity, expression patterns and percentage of stable transgene integration. Stable transgenic lines were established from selected founders.

2.6. Lipophilic dye labeling

Lipophilic dye labeling is a method that uses lipophilic dyes, such as DiI and DiO, to label the entire retinotectal projection in fixed zebrafish larvae. This technique was used in I*sl3:Gal4 10xUAS:rSyp-GCaMP6fEF05* and *Isl3:Gal4 10xUAS:rSyp-mCherry* fixed larvae. Lipophilic dye labeling was performed according to Hutson *et al.* 2004.

2.6.1. Preparation

Zebrafish larvae at 6 dpf were euthanized using 300 mg/L 3-amino benzoic acidethylester (tricaine) (composition in table II.6) and fixed overnight at 4°C with 4% paraformaldehyde (PFA). In the following day, the PFA solution was removed and the fixed larvae were washed with 1x Phosphate-Buffered Saline (PBS) (composition in table II.6).

Prior to injection, lipophilic dye solutions were prepared (1% (w/v) DiI (Sigma #42364) or DiO (Sigma #04292) in chloroform (Sigma #77619)) and injection needles were made with the same settings as the microinjection needles (Material and Methods, section 2.3.2).

2.6.2. Labeling

Zebrafish larvae were aligned in an agarose plate (1% (w/v) agarose in 1x PBS) and oriented in the lateral position after being embedded in low-melting agarose (1.5% (w/v) low-melting agarose

(Invitrogen #16520-050) in 1x PBS). Then, larvae were covered with 1x PBS. An injection needle was loaded with 2 µL of lipophilic dye solution and attached to the Pneumatic PicoPump PV 820. The pipette holder was held in a micromanipulator (Narishige, MN-153). The tip was broken using forceps.

Under a stereoscope, the lipophilic dye solution was injected in the gap between retina and lens (Figure II.2). The injected larvae were washed with 1x PBS and stored in the fridge until imaging.

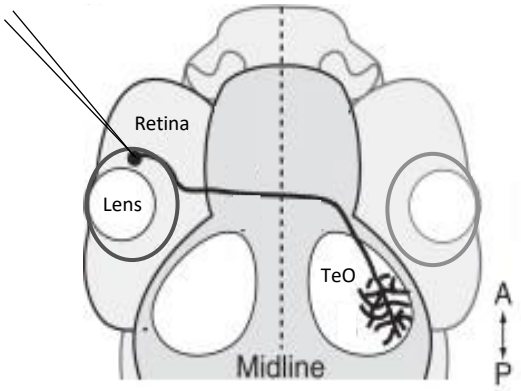

Figure II.2 – **Schematic representation of the lipophilic dye labeling.** Dorsal view of the head of a zebrafish larva, showing the injection of the lipophilic dye solution in the gap between retina and lens. Lipophilic dye labels the retinal ganglion cells which projecting in the optic tectum. TeO: optic tectum. A: anterior; P: posterior. Adapted from Poulain *et al*. 2010.

2.7. Confocal microscopy and image analysis

All zebrafish larvae used were firstly fixed in a PFA solution (Material and Methods, section 2.6.1). Fixed zebrafish larvae were mounted directly on a microscope slide (Menzel-Gläser, 76 x 26 mm), using 1.5% (w/v) low-melting agarose dissolved in 1x PBS. They were positioned as straight as possible in dorsal orientation. After the slide was surrounded by high vacuum grease (Dow corning) and filled with 1x PBS, a coverslip (Menzel-Gläser, 22 x 50 mm) was added. Zebrafish larvae injected with lipophilic dye solution were removed from the agarose plate in order to be mounted in the slide for imaging.

The images were obtained with the Zeiss LSM 710 fluorescence confocal microscope. For imaging, a 25x multi-immersion objective (N.A. 0.8) was used, as well as two lasers: 488 nm and 561 nm. Each slide was placed on the microscope stage and a drop of water was used as the immersion medium. Using the ZEN 2010 software, focal planes were selected and the acquisition parameters (gain, digital gain, digital offset and laser power) were optimized. The zebrafish larva brain was imaged in a stack format. All images were analyzed and treated in the open source software Fiji. For presentation purposes, Z-stack planes were selected, and maximum intensity projection was performed.

3. Solutions

Table II.6 – Summary of the composition of solutions used in this work. The solutions were prepared at Fish Platform or Glass Wash and Media Preparation Platform.

Working Solutions	Total volume and solvent	Composition
LB broth (Sterilized)	500 mL Milli-Q water	1.0% Bactotritone; 0.5% Yeast extract; 0.5% NaCl; pH 7.0 (adjusted with NaOH 5M)
LB broth agar plates (Sterilized)	500 mL LB broth	1.5% Bacto-agar
50x TAE (Stock Solution)	Fill to 1 L with Milli-Q water	242 g Trizma; 55.1 mL Acetic acid glacial 100 mL EDTA 0.5M (pH 8.0)
1x TAE	Fill to 500 mL with Milli-Q water	10 mL 50x TAE pH 8.0
1x TE	Fill to 100 mL with Milli-Q water	1 mL 1 M Tris base (pH 8.0) 0.2 mL EDTA 0.5M pH 8.0
50x E3 (Stock Solution)	2 L Milli-Q water	29.38 g NaCl; 1.26 g KCl; 4.86 g $CaCl_2.2H_2O$; 8,14 g $MgSO_4.7H_2O$
1x E3	Fill to 20 L with system water	400 mL 50x E3; 60 mL 0.01% Methylene Blue Solution (0.05 g Methylene Blue powder in 500 mL Milli-Q water)
E3-PhenolRed (Filtered)	15 mL 1x E3	0.0025% Phenol Red
25x Tricaine (Stock solution and Euthanasia)	10 mL 1 M Tris (1M Tris: 121.14 g Trizma base in 1 L reverse osmosis water; pH 9.0)	2 g tricaine powder; 500 mL reverse osmosis water; pH 7.0
1x PBS	1 L Milli-Q water	1.44g Na_2HPO_4; 0.24 g KH_2PO_4; 0.2 g KCl; 8 g NaCl; pH 7.2

III. Results

A key question in Neuroscience is to understand how the brain integrates sensory inputs and computes a behavioral output. The small size and transparency of zebrafish larvae in combination with the use of genetically encoded fluorescent reporters allow the non-invasive imaging of whole-brain neuronal activity and the study of neuronal circuits and their connectivity. In order to generate transgenic lines expressing genetically encoded fluorescent reporters, fluorescent reporter genes are cloned in plasmid DNA vectors, which are posteriorly injected into one-cell stage zebrafish embryos.

In this work, we constructed two types of expression clones: UAS expression clones, harboring a 10xUAS regulatory sequence, and *alpha-1-Tubulin* expression clones, harboring the *alpha-1-Tubulin* putative promoter. Both were generated with two different genetically encoded fluorescent reporter genes: *LSSmOrange* and *mScarlet.* The expression clones were then injected into one-cell stage *Isl3:Gal4*$^{+/+}$ transgenic or *nacre*$^{+/-}$ zebrafish embryos to create stable transgenic lines.

1. Construction of UAS expression clones

In order to generate 10xUAS expression clones, we used the Gateway cloning technology (Figure III.1), since it provides a rapid and highly efficient way to transfer one or more DNA fragments into multiple vectors, maintaining the orientation and reading frame (Hartley *et al.* 2000).

Through LR recombination reaction an entry clone containing 10 repetitions of the UAS sequence (10xUAS) was recombined with a destination vector. Destination vectors were constructed by cloning of *LSSmOrange* and *mScarlet* genes into an empty *Tol2* Gateway destination vector, that contained *Tol2* arms required for transposition in zebrafish embryos, upon microinjection.

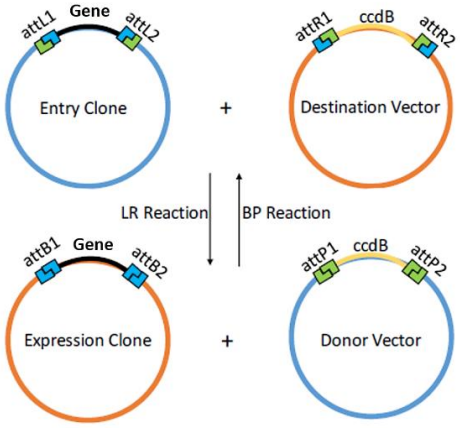

Figure III.1 – Gateway recombinant system. The key of the gateway cloning technology is the site-specific attachment (*att*) sites, which recombine in a direction and site-specific manner, depending on the recombination reactions. The gateway cloning technology includes two recombination reactions: LR reaction and BP reaction. The LR reaction is a recombination reaction between an entry clone and a destination vector, to create an expression clone. This reaction occurs between *att*L and *att*R sites and is catalyzed by the LR Clonase enzyme mix. The BP reaction is the reverse of the LR reaction. The BP reaction transfers the gene in the expression clone into a donor vector, to produce a new entry clone. The recombination reaction is catalyzed by the BP Clonase enzyme mix and occurs between *att*B and *att*P sites. The *ccdB* is a toxic gene used in bacterial cell selection. Adapted from Gateway Technology User Guide, Invitrogen.

1.1. Strategy used for the construction of pDestTol2-LSSmOrange and pDestTol2-mScarlet vectors

In order to construct the destination vectors: pDestTol2-LSSmOrange (Supplement A.8A) and pDestTol2-mScarlet (Supplement A.8B), fluorescent reporter genes were isolated by PCR from two commercial vectors: pH2B-LSSmOrange and pmScarlet_C1. *LSSmOrange* and *mScarlet* genes were amplified using primers (Table II.2 and Table III.1) with specific restriction sites and a functional Kozak sequence upstream of the ATG of the gene of interest. PCR products were separated through agarose gel electrophoresis and posteriorly extracted from agarose gel. PCR fragments and *Tol2* Gateway destination vector (backbone) were digested with appropriate restriction endonucleases (Table II.3), creating compatible cohesive ends for ligation of the backbone with PCR-digested products (Figure III.2).

Table III.1 – Primers used for the amplification and subsequent cloning of *LSSmOrange* and *mScarlet* genes into a *Tol2* Gateway destination vector.

Primer	Template	Target	Ta (°C) [(a)]	DNA Polymerase	DNA fragment size (bp)
SpeI-kz-LSSmOrange_Fw	pH2B-LSSmOrange	*LSSmOrange*	68.3	Phusion DNA Polymerase	735
PacI-Stop-LSSmOrange_Rv					
SpeI-kz-mScarlet_Fw	pmScarlet_C1	*mScarlet*	67.2	Phusion DNA Polymerase	723
PacI-Stop-mScarlet_Rv					

[(a)] Working annealing temperature (Ta): Annealing temperature – 0.5°C.

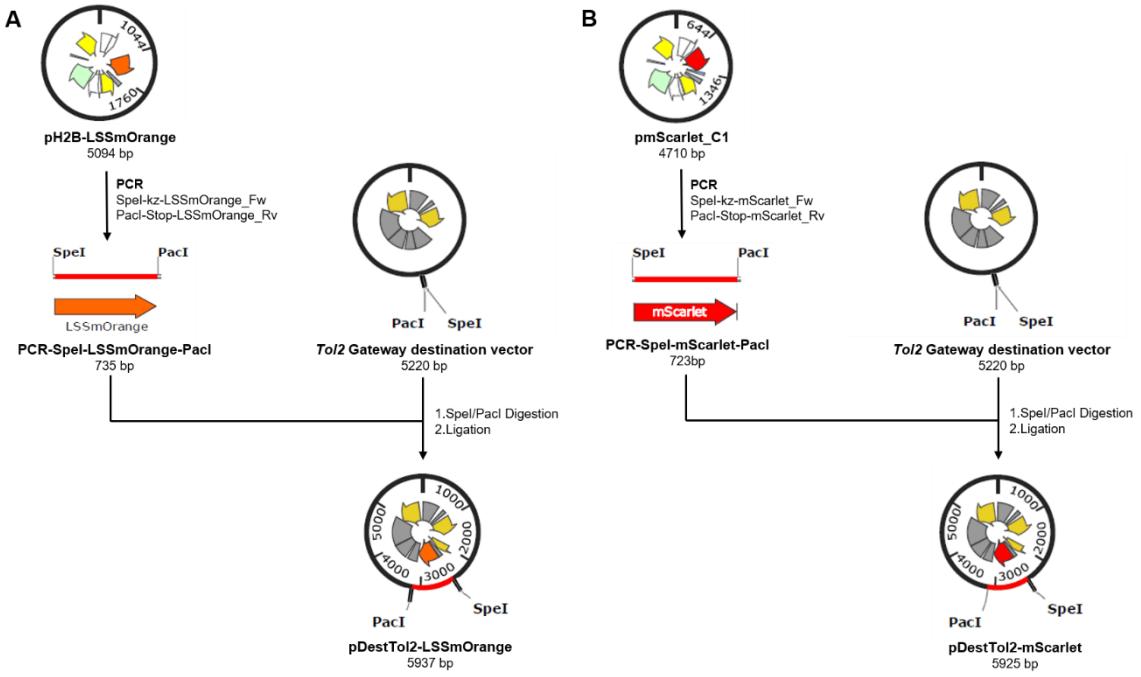

Figure III.2 – General cloning strategy for the construction of the destination vectors. Fluorescent reporter genes were isolated from original plasmid by PCR with primers designed to have *SpeI* and *PacI* restriction sites flanking the PCR product. PCR fragments were cloned into a *Tol2* Gateway destination vector containing the same restriction sites. Cloning strategy of pDestTol2-LSSmOrange **(A)** and pDestTol2-mScarlet **(B)** vectors**.**

To confirm successful cloning, pDestTol2-LSSmOrange and pDestTol2-mScarlet vectors were digested with restriction endonucleases (*BstXI* and *NotI,* respectively). Restriction profiles were analyzed on agarose gel (Figure III.3A-B) and correct sequence was confirmed by sequencing.

pDestTol2-LSSmOrange vector was expected to be cut 3 times by *BstXI* restriction endonuclease, originating 3 bands in the agarose gel with 724 bp, 1455 bp and 3758 bp. As shown in the figure III.3A, only clone #1 has the expected size and number of fragments. pDestTol2-mScarlet vector was expected to be cut twice by *NotI* restriction endonuclease, originating 2 bands in the agarose gel with 2104 bp and 3821 bp. As shown in the figure III.3B, only the clones #1 and #4 are positive for the presence of the insert.

Positive clones were sequenced, and the resulting sequences were compared against the expected ones, using SnapGene (Figure III.3C-D). Figure III.3C-D confirms the presence of the *LSSmOrange* and *mScarlet* genes into the *Tol2* Gateway destination vector and the absence of mutations in these genes, potentially introduced by the DNA Polymerase in the PCR.

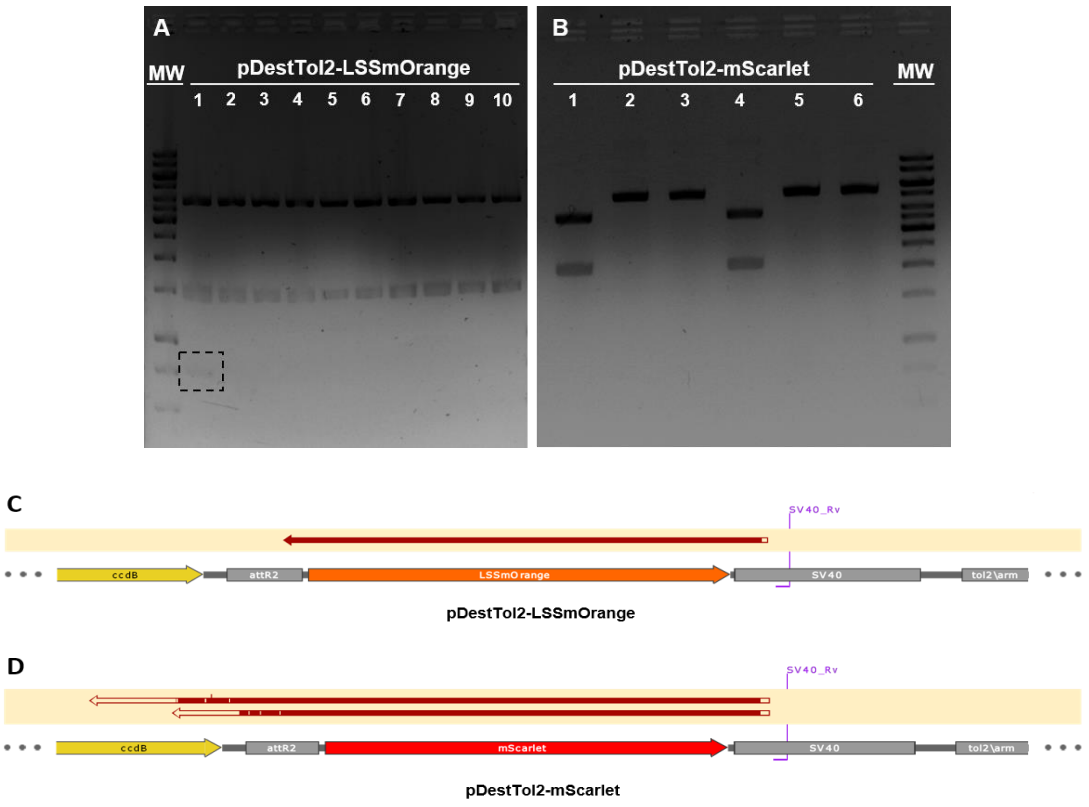

Figure III.3 – Restriction profiles on agarose gel and sequencing results of the destination vectors. **(A)** Restriction profile of digested pDestTol2-LSSmOrange vector with *BstXI* restriction endonuclease. The dashed box represents the faint band of 724 bp. **(B)** Restriction profile of digested pDestTol2-mScarlet vector with *NotI* restriction endonuclease. Lane MW: molecular weight ladder, GeneRuler 1 Kb DNA ladder (Supplement A.3). **(C-D)** Comparison of sequencing results (top red arrows) of pDestTol2-LSSmOrange clone #1 **(C)** and pDestTol2-mScarlet clones #1 and #4 **(D)** against the expected sequence, using SnapGene. In both cases, SV40_Rv primer (Table II.4) was used for sequencing.

1.2. Strategy used for the construction of pTol2-10xUAS-LSSmOrange and pTol2-10xUAS-mScarlet expression clones

In order to generate pTol2-10xUAS-LSSmOrange (Supplement A.9A) and pTol2-10xUAS-mScarlet (Supplement A.9B) expression clones, a LR recombination reaction was performed between the destination vectors constructed and a preexistent 10xUAS entry clone (Figure III.4).

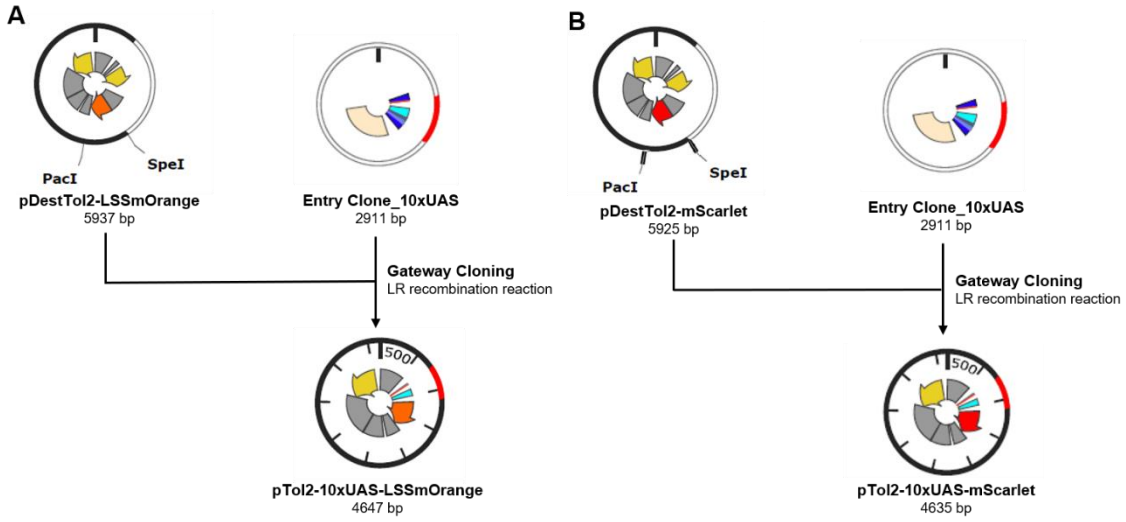

Figure III.4 – General cloning strategy for the construction of the 10xUAS expression clones. Recombination between the destination vectors previously constructed and an entry clone with the 10xUAS regulatory sequence, through LR recombination reaction. Cloning strategy of the pTol2-10xUAS-LSSmOrange **(A)** and pTol2-10xUAS-mScarlet **(B)** expression clones.

To confirm successful cloning, pTol2-10xUAS-LSSmOrange and pTol2-10xUAS-mScarlet vectors were digested with *SacI-HF* restriction endonuclease. Restriction profiles were analyzed on agarose gel (Figure III.5A-A') and correct sequence was confirmed by sequencing.

Both vectors were expected to have 2 sites of recognition by *SacI-HF* restriction endonuclease, originating 2 bands in agarose gel. That way, bands of 809 bp and 3838 bp were expected for pTol2-10xUAS-LSSmOrange and bands of 797 bp and 3838 bp for pTol2-10xUAS-mScarlet. As shown in figure III.5A-A', all clones have the expected size and number of fragments.

Only one clone of each expression clone was selected to be sequenced. The resulting sequences were compared against the expected ones, using SnapGene (Figure III.5B-C). The sequencing confirms the absence of mutations in *LSSmOrange* and *mScarlet* genes. Upon confirmation of the correct sequence, the expression vectors were purified for posterior injection in *Isl3:Gal4*$^{+/+}$ transgenic embryos.

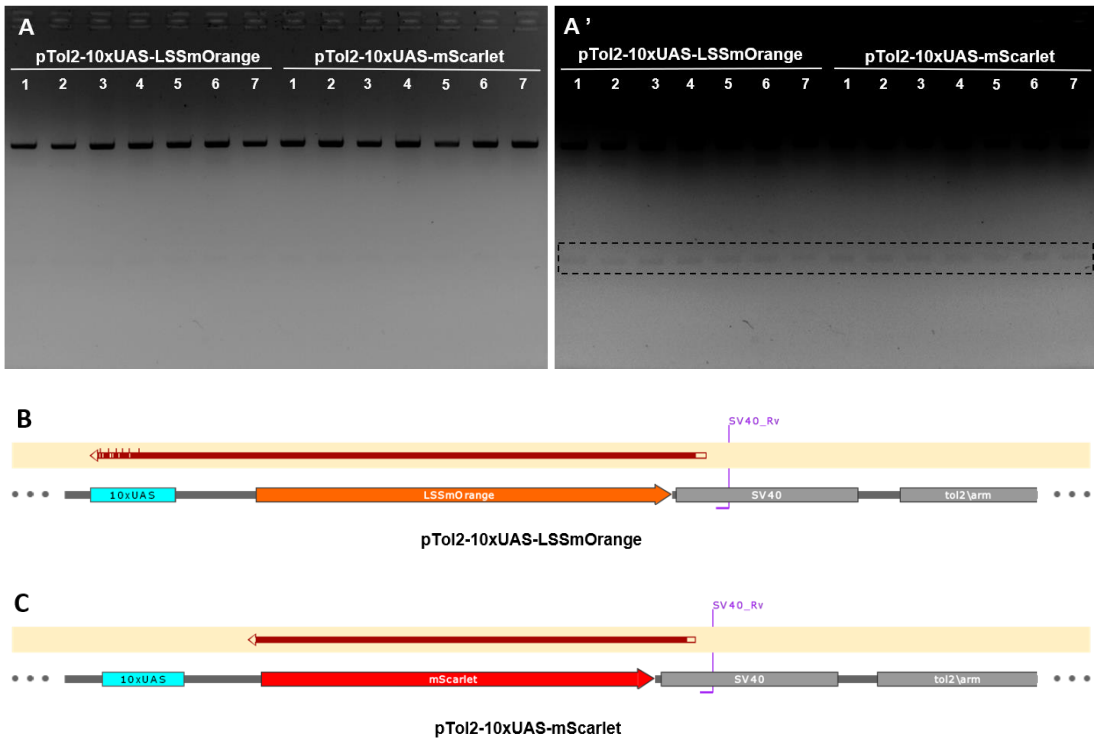

Figure III.5 – **Restriction profiles on agarose gel and sequencing results of the 10xUAS expression clones. (A-A')** Restriction profile of the digested pTol2-10xUAS-LSSmOrange and pTol2-10xUAS-mScarlet expression clones with *SacI-HF* restriction endonuclease. The dashed box represents the low molecular weight faint bands. Although the molecular weight ladder is not visible, it was used GeneRuler 1 Kb DNA ladder (Supplement A.3). Photo of the restriction profile with low **(A)** and high **(A')** exposure for better visualization of faint bands. **(B-C)** Comparison of sequencing results (top red arrows) of pTol2-10xUAS-LSSmOrange clone #3 **(B)** and pTol2-10xUAS-mScarlet clone #3 **(C)** against the expected sequence, using SnapGene. In both cases, SV40_Rv primer (Table II.4) was used for sequencing.

2. Construction of *alpha-1-Tubulin* expression clones

In order to generate *alpha-1-Tubulin* expression clones we performed Gibson Assembly to seamlessly join two fragments: *alpha-1-Tubulin* putative promotor and fluorescent reporter gene. Gibson Assembly is an efficient and robust cloning procedure that allows assembling multiple overlapping DNA fragments (Figure III.6A), regardless of fragment length or end compatibility (Gibson *et al.* 2009).

The assembled fragments were cloned into a pCR2.1-TOPO TA vector, by means of TA Cloning (Figure III.6B). After subcloning into the pCR2.1-TOPO vector, the assembled fragments were then cloned into a *Tol2* vector, since *Tol2* arms are required for transposition in zebrafish embryos, upon microinjection.

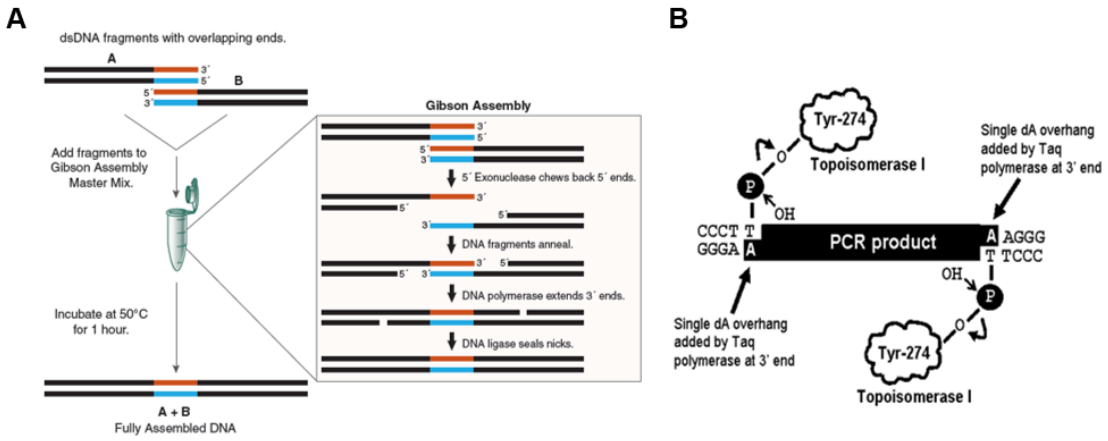

Figure III.6 – Molecular cloning methods. (A) Gibson Assembly method. The Gibson Assembly is a single-tube isothermal reaction, using a Gibson Assembly Master Mix, which contains three different enzymatic activities. First, an exonuclease cuts back the 5' ends of the overlapping nucleotides (red and blue), to create single-stranded 3' overhangs. These overhangs facilitate the annealing of complementary fragments (overlap region). Secondly, a DNA polymerase extends the 3' ends to fill the gaps in annealed products and last a DNA ligase seals the nicks in the assembled DNA. For that, DNA fragments are added to the master mix and incubated at 50°C for 1 hour. The final product is a fully ligated double-stranded DNA. Adapted from Gibson Assembly Master Mix Instruction Manual, NEB. **(B) TA cloning method.** TA cloning is an efficient method for the cloning of PCR products. Taq polymerase adds a single 3'-A overhang to each end of the PCR products, by the enzyme's terminal transferase activity. The use of a linearized TOPO TA vector with a single 3'-T overhang on both ends allows direct cloning of PCR products, which is facilitated by complementarity between the PCR product 3'-A overhangs and vector 3'-T overhangs. Ligation of the PCR product to the vector is carried out by the enzyme Topoisomerase I. Adapted from TOPO TA Cloning Kit User Guide, Invitrogen.

2.1. Strategy used for the construction of pTol2-alpha1Tubulin-LSSmOrange and pTol2-alpha1Tubulin-mScarlet expression clones

In order to construct pTol2-alpha1Tubulin-LSSmOrange (Supplement A.10A) and pTol2-alpha1Tubulin-mScarlet vectors (Supplement A.10B), the fluorescent reporter genes and the *alpha-1-Tubulin* putative promotor were isolated by PCR from destination vectors (Results, section 1.1) and pT-alpha1Tubulin-GCaMP vector, respectively. Fluorescent reporter genes were amplified using primers with specific restriction sites and an overlapping region with 3' end of the *alpha-1-Tubulin* fragment (Table II.2, Table III.2); *alpha-1-Tubulin* putative promotor was amplified using primers with specific restriction sites and an overlapping region with 5' end of the fluorescent report fragment (Table II.2, Table III.2). The *alpha-1-Tubulin* fragment was fused with each fluorescent reporter fragment by means of Gibson Assembly.

To increase fragment yield and ensure the presence of the full *alpha-1-Tubulin*-fluorescent reporter fragment, the assembled products were amplified by PCR, using the external primers (Table II.2, Table III.2). PCR products were cloned into the pCR2.1-TOPO TA vector, by means of TA Cloning (Figure III.7). PCR products can be inserted randomly in either orientation from 5' to 3' or from 3' to 5'.

Table III.2 – Primers used for the amplification of *alpha-1-Tubulin*, *LSSmOrange* and *mScarle*t fragments and primers used for the amplification and subsequent cloning of the assembled products into the pCR2.1-TOPO TA vector.

Primer	Template	Target	Ta (°C) [a]	DNA Polymerase	DNA fragment size (bp)
EcoRI-α1Tubpromoter_Fw	pT-alpha1Tubulin-GCaMP	*alpha-1-Tubulin*	72.0	Platinum DNA Polymerase	2713
α1TubuIntron1-LSSmOrange/mScarlet_Rv					
α1Tubpromoter-(No ATG)-LSSmOrange_Fw	pDestTol2-LSSmOrange	*LSSmOrange*	69.6	Phusion DNA Polymerase	734
PacI-Stop-LSSmOrange_Rv					
α1Tubpromoter-(No ATG)-mScarlet_Fw	pDestTol2-mScarlet	*mScarlet*	68.0	Phusion DNA Polymerase	722
PacI-Stop-mScarlet_Rv					
EcoRI-α1Tubpromoter_Fw	*alpha-1-Tubulin-LSSmOrange* Assembly	*alpha-1-Tubulin-LSSmOrange* Assembly	71.5	Phusion DNA Polymerase	3419
PacI-Stop-LSSmOrange_Rv					
EcoRI-α1Tubpromoter_Fw	*alpha-1-Tubulin-mScarlet* Assembly	*alpha-1-Tubulin-mScarlet* Assembly	71.5	Phusion DNA Polymerase	3408
PacI-Stop-mScarlet_Rv					

[a] To optimize the PCR and reduce nonspecific PCR products, a temperature gradient was performed. The represented annealing temperature (Ta) corresponds to the temperature used for amplification.

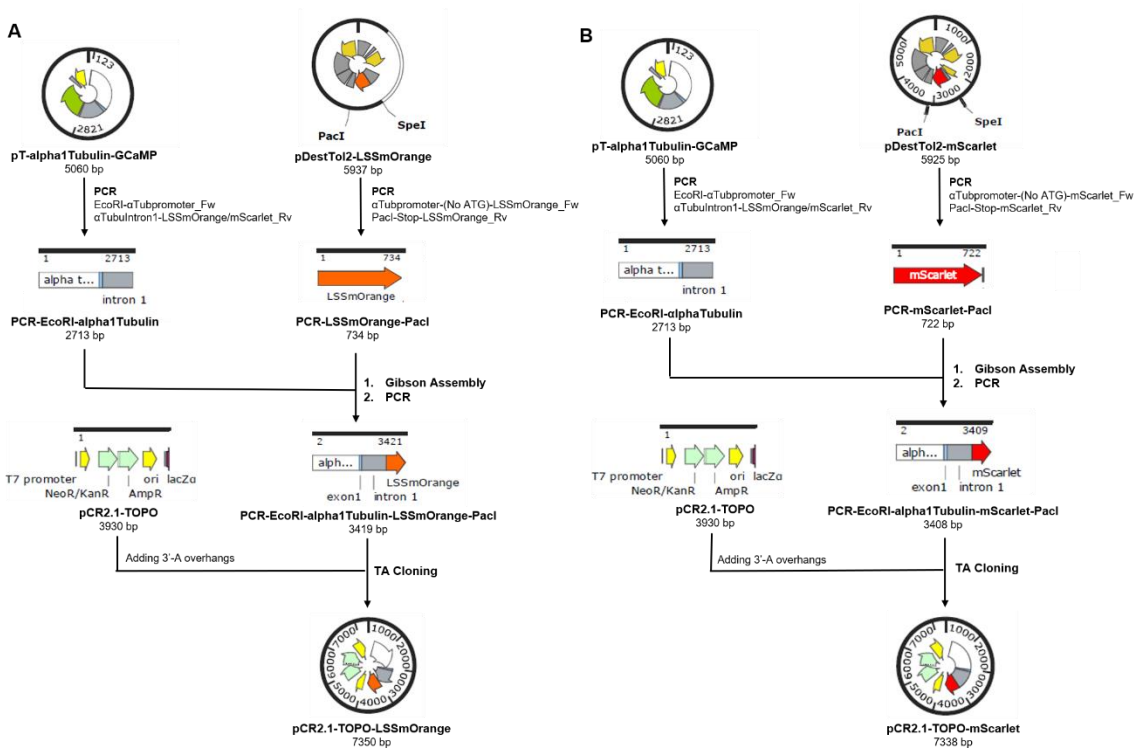

Figure III.7 – General cloning strategy for the construction of the intermediate vectors. Fluorescent reporter genes and *alpha-1-Tubulin* putative promotor were isolated by PCR from destination vectors and original plasmid, respectively. *alpha-1-Tubulin* fragment was fused with fluorescent reporter gene, by Gibson Assembly. The assembled fragments were cloned into a pCR2.1-TOPO TA vector, by TA Cloning. Cloning strategy of the pCR2.1-TOPO-LSSmOrange **(A)** and pCR2.1-TOPO-mScarlet **(B)** intermediate vectors.

To confirm successful cloning, pCR2.1-TOPO-LSSmOrange and pCR2.1-TOPO-mScarlet intermediate vectors were digested with restriction endonucleases (*SacI-HF* and *NotI,* respectively). Restriction profiles were analyzed on agarose gel (Figure III.8A-B) and correct sequence was confirmed by sequencing.

pCR2.1-TOPO-LSSmOrange intermediate vector was expected to be cut twice by *SacI-HF* restriction endonuclease: bands of 1800 bp and 5550 bp (if orientation of insert is 5' to 3') or bands of 1711 bp and 5639 bp (if insert orientation is 3' to 5') should be observed in the agarose gel. As shown in figure III.8A, clones #1 and #2 have the expected size and number of fragments. pCR2.1-TOPO-mScarlet intermediate vector was expected to be cut twice by *NotI* restriction endonuclease: bands of 230 bp and 7108 bp (if orientation of insert is 5' to 3') or bands of 3249 bp and 4089 bp (if insert orientation is 3' to 5') should be observed in the agarose gel. As shown in figure III.8B, clones #1 and #2 have the expected size and number of fragments.

Positive clones were sequenced, and the resulting sequences were compared against the expected ones, using SnapGene (Figure III.8C-D). Figure III.8C-D confirms the assembly between *alpha-1-Tubulin* and fluorescent reporter fragments, but also shows the presence of mutations in *alpha-1-Tubulin* fragment, that might have been introduced by the DNA Polymerase in PCR.

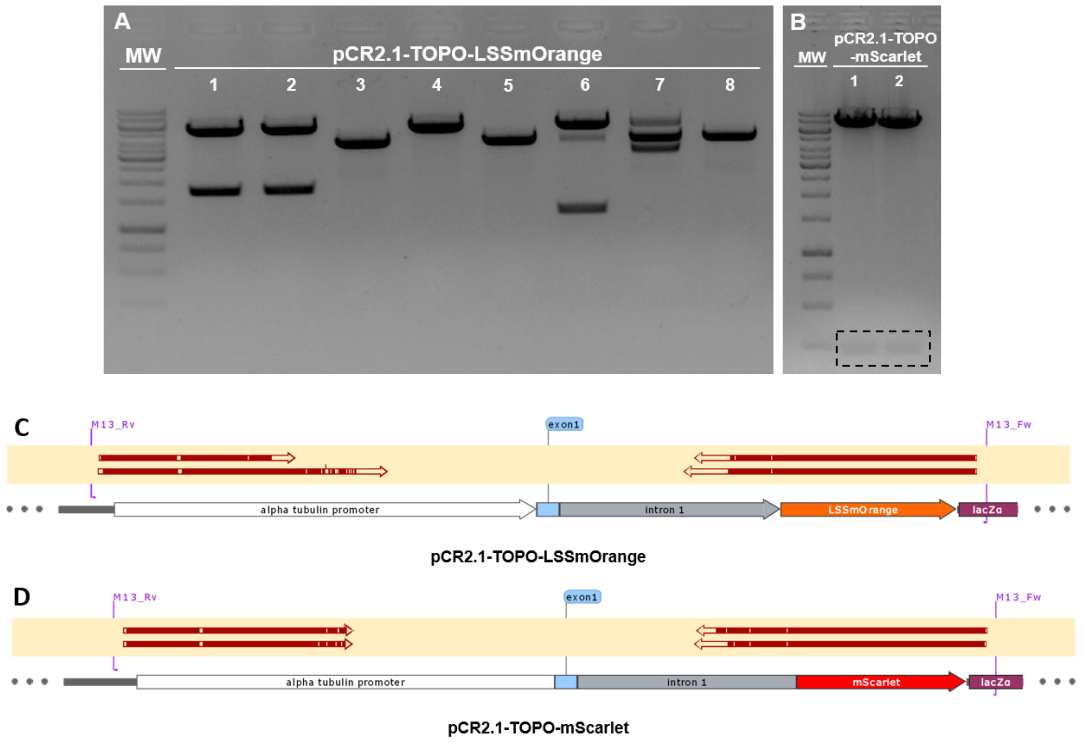

Figure III.8 – Restriction profiles on agarose gel and sequencing results of the pCR2.1-TOPO intermediate vectors. (A) Restriction profile of the digested pCR2.1-TOPO-LSSmOrange intermediate vector with *SacI-HF* restriction endonuclease. **(B)** Restriction profile of digested pCR2.1-TOPO-mScarlet intermediate vector with *NotI* restriction endonuclease. The dashed box represents the faint band of 230 bp. Lane MW: molecular weight ladder, GeneRuler 1 Kb DNA ladder (Supplement A.3). **(C-D)** Comparison of sequencing (top red arrows) results of pCR2.1-TOPO-LSSmOrange clones #1 and #2 **(C)** and pCR2.1-TOPO-mScarlet clones #1 and #2 **(D)** against the expected sequence, using SnapGene. In both cases, M13_Fw and M13_RV primers (Table II.4) were used for sequencing.

After TA cloning, the assembled fragments should have been directly cloned into the pDestTol2-LSSmOrange vector (backbone). However, the mutations present in *alpha-1-Tubulin* fragment led to an additional step, in order to replace the mutated sequence by an *alpha-1-Tubulin* sequence that it knows beforehand to be correct – the sequence present in original plasmid (pT-alpha1Tubulin-GCaMP). This was done by cutting vectors with the same unique enzymes, therefore replacing the mutated sequence with a non-mutated one (Figure III.9).

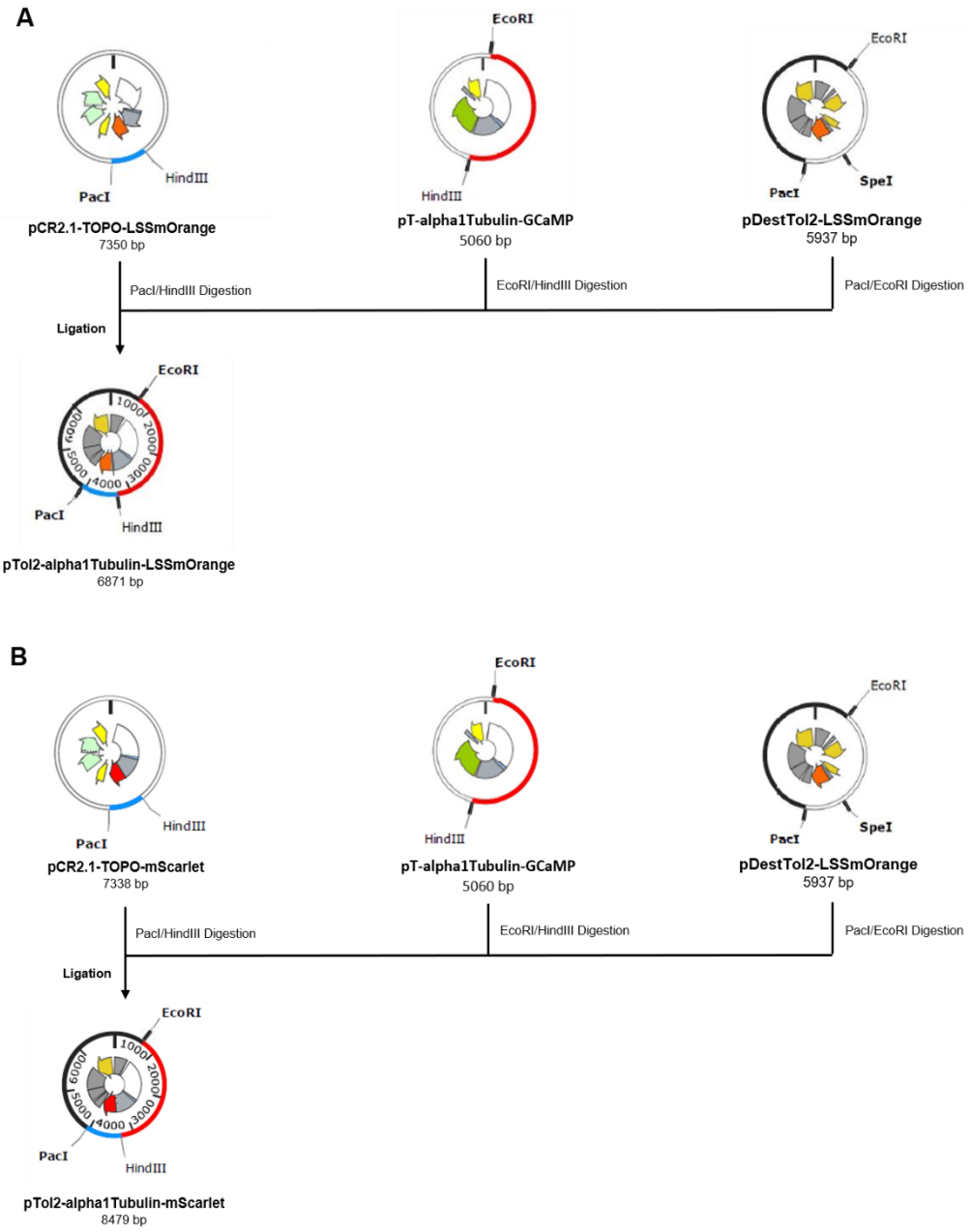

Figure III.9 – Restriction digestions for the construction of pTol2-alpha1Tubulin-LSSmOrange and pTol2-alpha1Tubulin-mScarlet expression clones. Restriction digestion of the pCR2.1-TOPO intermediate vectors with *HindIII* and *PacI* restriction endonucleases to isolate the end of the *alpha-1-Tubulin*-fluorescent reporter assembly fragment; restriction digestion of the alpha1Tubulin-GCaMP vector with *HindIII* and *EcoRI* restriction endonucleases to isolate *alpha-1-Tubulin* fragment; restriction digestion of the pDestTol2-LSSmOrange vector with *EcoRI* and *PacI* restriction endonucleases to isolate the backbone used in final vectors. All fragments were united by T4 DNA ligase. Restriction digestions for the construction of the pTol2-alpha1Tubulin-LSSmOrange **(A)** and pTol2-alpha1Tubulin-mScarlet **(B)** expression clones.

To confirm successful cloning, pTol2-alpha1Tubulin-LSSmOrange and pTol2-alpha1Tubulin-mScarlet vectors were digested with *SacI-HF* and *PstI* restriction endonucleases. Restriction profiles were analyzed on agarose gel (Figure III.10A-B) and correct sequence was confirmed by sequencing.

pTol2-alpha1Tubulin-LSSmOrange vector was expected to be cut 3 times by *SacI-HF* and *PstI* restriction endonucleases, creating 3 fragments seen as 3 bands in agarose gel with 1662 bp, 1985 bp and 3212 bp. As shown in figure III.10A-A', all clones have the expected size and number of fragments. pTol2-alpha1Tubulin-mScarlet vector was expected to be cut 4 times by *SacI-HF* and *PstI* restriction endonucleases, creating 4 fragments seen as 4 bands in the agarose gel with 376 bp, 1298 bp, 1985 bp and 3214 bp. As shown in figure III.10B, all clones are positive.

Only one clone of each expression clone was selected to be sequenced. The resulting sequences were compared against the expected ones, using SnapGene (Figure III.10C-D). Figure III.10C-D confirms the absence of mutations in *alpha-1-Tubulin*-fluorescent reporter assembly fragments. Upon confirmation of the correct sequences, the expression vectors were purified for posterior injection in *nacre*$^{+/-}$ zebrafish embryos.

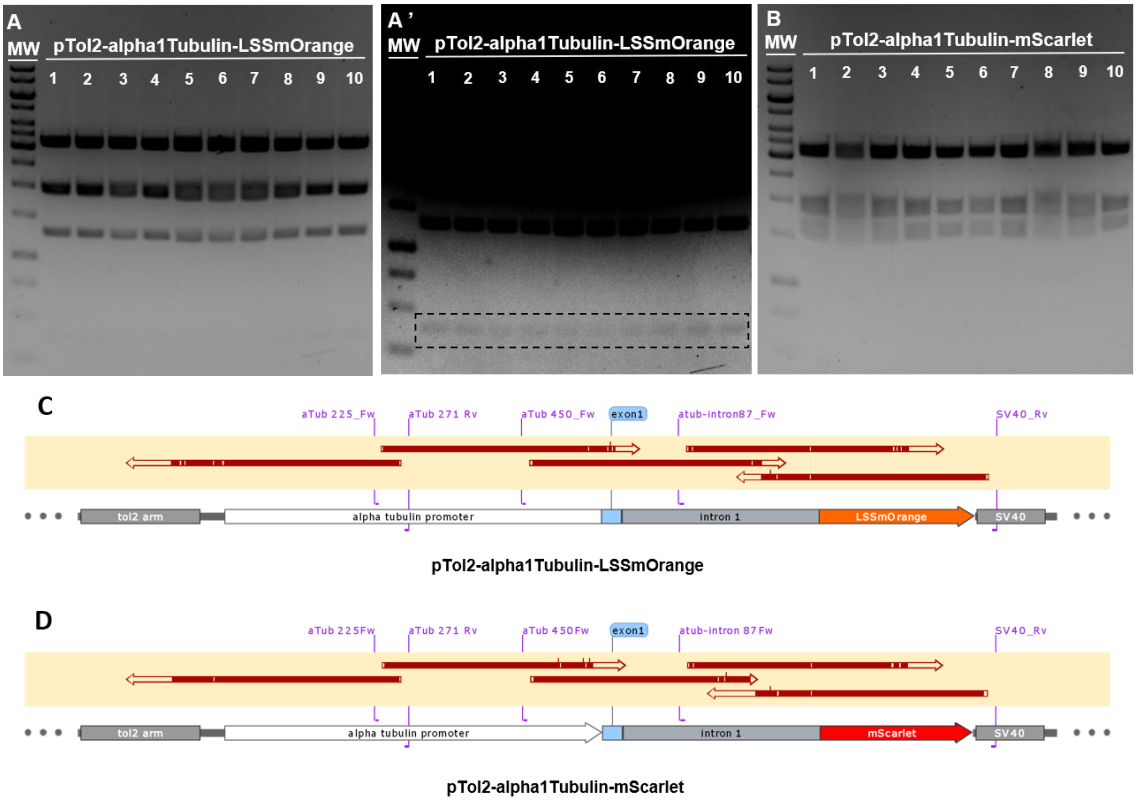

Figure III.10 – Restriction profiles on agarose and sequencing results of the *alpha-1-Tubulin* expression clones. (A) Restriction profile of the digested pTol2-alpha1Tubulin-LSSmOrange vector with *SacI-HF* and *PstI* restriction endonucleases. The dashed box represents the low molecular weight faint bands. Photo of the restriction profile with low **(A)** and high **(A')** exposure for better visualization of faint bands. **(B)** Restriction profile of the digested pTol2-alpha1Tubulin-mScarlet vector with *SacI-HF* and *PstI* restriction endonucleases. Lane MW: molecular weight ladder, GeneRuler 1 Kb DNA ladder (Supplement A.3). **(C-D)** Comparison of sequencing results (top red arrows) of pTol2-alpha1Tubulin-LSSmOrange clone #2 **(C)** and pTol2-alpha1Tubulin-mScarlet clone #4 **(D)** against the expected sequence, using SnapGene. In both cases α1Tub225_Fw, α1Tub450_Fw, α1Tub-intron87_Fw, α1Tub271_Rv and SV40_Rv primers (Table II.4) were used for sequencing.

3. Generation and characterization of transgenic zebrafish lines

After the construction of the expression clones, plasmid DNA vectors were prepared for microinjection in zebrafish embryos, in order to generate transgenic zebrafish lines. The expression clones were injected into one-cell stage *Isl3:Gal4*$^{+/+}$ transgenic (10xUAS expression clones) and *nacre*$^{+/-}$ embryos (*alpha-1-Tubulin* expression clones).

The Tg (*Isl3:Gal4*$^{+/+}$) driver line exhibits an Isl3 expression pattern, which is characterized by expression in RGCs, hindbrain, optic tectum, trigeminal nerve, spinal cord and habenula (Figure III.11) (Thisse & Thisse 2004; Renninger *et al.* 2011), when a UAS-coupled genetically encoded fluorescent reporter gene is present, either by crossing it with a reporter line or injection of an UAS expression clone.

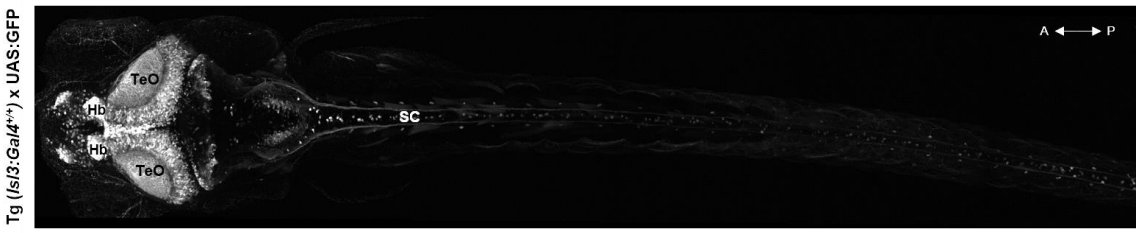

Figure III.11 – Expression pattern of the Tg (*Isl3:Gal4*$^{+/+}$) driver line. Confocal microscope image of dorsal view of an *Isl3:Gal4*$^{+/+}$ zebrafish larva at 6 dpf. Tg (*Isl3:Gal4*$^{+/+}$) driver line exhibits an Isl3 expression pattern driven by the *isl3* promoter. Retinal ganglion cells (RGCs), hindbrain and trigeminal nerve are not visible. Hb: habenula; SC: spinal cord; TeO: optic tectum. A: Anterior; P: Posterior.

Two other expression clones (pTol2-10xUAS:rSyp-mCherry and pTol2-10xUAS:rSyp-GCaMP6fEF05), previously cloned by Michael Orger's Laboratory, were also injected into one-cell stage *Isl3:Gal4*$^{+/+}$ transgenic embryos, in order to establish transgenic lines for the study of the neuronal connectivity and neuronal activity in zebrafish.

3.1. Transient expression of the fluorescent reporter genes

Following the microinjection of the expression clones (Table II.5), injected embryos at 2-3 dpf were pre-screened for transient expression of the respective fluorescent reporter gene (Table III.3), in order to examine if the promoter would be capable to drive fluorescent reporter expression to predictable tissues.

The *Isl3:Gal4*$^{+/+}$ transgenic embryos injected with 10xUAS expression clones exhibited a characteristic Isl3 expression pattern (Figure III.12A-C) and the nacre$^{+/-}$ embryos injected with pTol2-alpha1Tubulin-mScarlet expression clone exhibited a pan-neuronal expression pattern (Figure III.12D). As expected from transient expression, the Isl3 expression pattern was not complete (Figure III.12A-C), since it was only visible fluorescence in trigeminal nerve and spinal cord. Injected larvae with 10xUAS expression clones also exhibited different levels of brightness between them (data not shown). Thus, to establish a transgenic zebrafish line we selected to raise into adulthood the larvae with high fluorescence intensity and a complete trigeminal nerve expression pattern.

Injected larvae with pTol2-alpha1Tubulin-mScarlet expression clone exhibited high fluorescence intensity and a close to complete pan-neuronal expression pattern. Thus, the selection of larvae to be raise into adulthood was random within the positive larvae.

Table III.3 – Screening results of each transgenic zebrafish line generated.

Transgenic zebrafish line	Injected fish raised	Injected fish screened	Positive screened fish	% of positive screened fish [(a)]	% of Δ stable integration [(b)]
Isl3:Gal4 10xUAS:rSyp-mCherry	100	69	38	55%	0.60-66%
Isl3:Gal4 10xUAS:rSyp-GCaMP6fEF05	36	29	22	76%	0.60-77%
Isl3:Gal4 10xUAS-mScarlet	69	10	6	60%	0.40-74%
alpha1Tubulin-mScarlet	23	17	9	64%	0.50-61%

(a) # Positive screened fish / # Injected fish screened x 100
(b) # Positive F0 larvae / # F0 larvae screened x 100

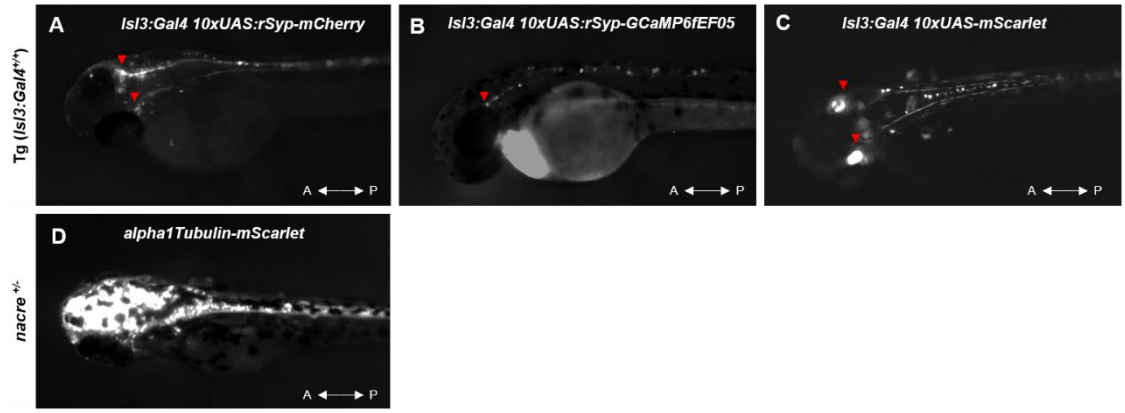

Figure III.12 – Transient expression of the microinjected constructs' fluorescent reporter genes in one-cell stage *Isl3:Gal4*$^{+/+}$ and *nacre*$^{+/-}$ zebrafish embryos. Injected embryos were screened at 2-3 dpf, using Zeiss StrREO Discovery.V8 scope. **(A-C)** *Isl3:Gal4 10xUAS-GOI* (gene of interest) representative zebrafish larvae with partial Isl3 expression pattern. Red arrow points to trigeminal ganglion, that projects to the spinal cord**.** *Isl3:Gal4 10xUAS:rSyp-mCherry* **(A)** *Isl3:Gal4 10xUAS:rSyp-GCaMP6fEF05* **(B)** and *Isl3:Gal4 10xUAS-mScarlet* **(C)** representative transgenic zebrafish larvae. **(D)** *alpha1Tubulin-mScarlet* representative zebrafish larva with pan-neuronal expression pattern. A: anterior; P: posterior.

3.2. Stable expression of the fluorescent reporter genes and characterization of zebrafish lines

When the positive injected zebrafish reached sexual maturity, they were crossed with the same zebrafish lines used for the microinjection, in order to identify which of them integrated the transgene in germ cells and transmitted it to the progeny. For that, the progeny (F0 generation) was screened for stable expression of the respective fluorescent reporter gene.

In the stable expression screen, the progeny of injected fish with 10xUAS expression clones showed a mosaic heterogeneous expression (data not shown), since the larvae exhibited different levels of fluorescent intensity and different expression patterns. Thus, to establish a stable

transgenic zebrafish line, we selected the larvae with high fluorescence intensity and a complete trigeminal nerve expression pattern. Moreover, within the positive injected zebrafish which progeny show similar expression, we have chosen the ones with a high integration efficiency and low percentage of stable transgene integration (Table III.3), which will potentially be translated into a single event of integration in the genome.

On the other hand, the positive progeny from injected fish with pTol2-alpha1Tubulin-mScarlet expression clone did not exhibit a mosaic heterogeneous expression. The larvae were selected to grow based on the same parameters that the progeny from injected fish with 10xUAS expression clones, but for the pan-neuronal expression pattern.

To characterize the expression of fluorescent reporter genes and/or confirm its correct expression in the transgenic lines generated, a small representative number of positive embryos were selected and grown until 6 dpf for further imaging at the confocal microscope. To confirm *Isl3:Gal4 10xUAS:rSyp-mCherry* and *Isl3:Gal4 10xUAS:rSyp-GCaMPEF05* correct expression, it was necessary to perform a lipophilic dye labeling (Hutson *et al.* 2004) previous to imaging.

3.2.1. *Isl3:Gal4 10xUAS:rSyp-mCherry* line

From the 100 *Isl3:Gal4 10xUAS:rSyp-mCherry* injected fish that were selected to reach sexual maturity, 69 of them were screened for stable expression. It was estimated that 55% (38/69) of screened fish (Table III.3) contained at least a stable integration of the pTol2-10xUAS:rSyp-mCherry vector in germ cells, since the progeny exhibited a characteristic Isl3 expression pattern (Figure III.13A-B''). The percentage of stable transgene integration in the screened population varied between 0.60% and 66% (Table III.3). To establish a stable transgenic line, the progeny from zebrafish with lower percentage of stable transgene integration in germ cells was selected to be raised until adulthood.

In order to characterize the fluorescent reporter expression and confirm its correct expression, a small number of F0 positive embryos with 6 dpf was fixed in a PFA solution and imaged at the confocal microscope. As shown in figure III.13A-B'', the *Isl3:Gal4 10xUAS:rSyp-mCherry* zebrafish line displays a characteristic Isl3 expression pattern with the *isl3* promoter driving mCherry expression to the cells of trigeminal ganglion, optic tectum and spinal cord.

To confirm the expression of the mCherry in presynaptic vesicles of the structures labeled by the *isl3* promoter we performed the anterograde labeling of RGCs' axon terminals with the lipophilic dye, DiO (green) (Figure III.13C''). Since the RGC axons are projected in the optic tectum, it is possible to visualize the synaptic connections (yellow) between their neurons (Figure III.13C'''), which suggest that the expression of mCherry is being targeted to presynaptic vesicles of cells that correspond to the Isl3 expression pattern.

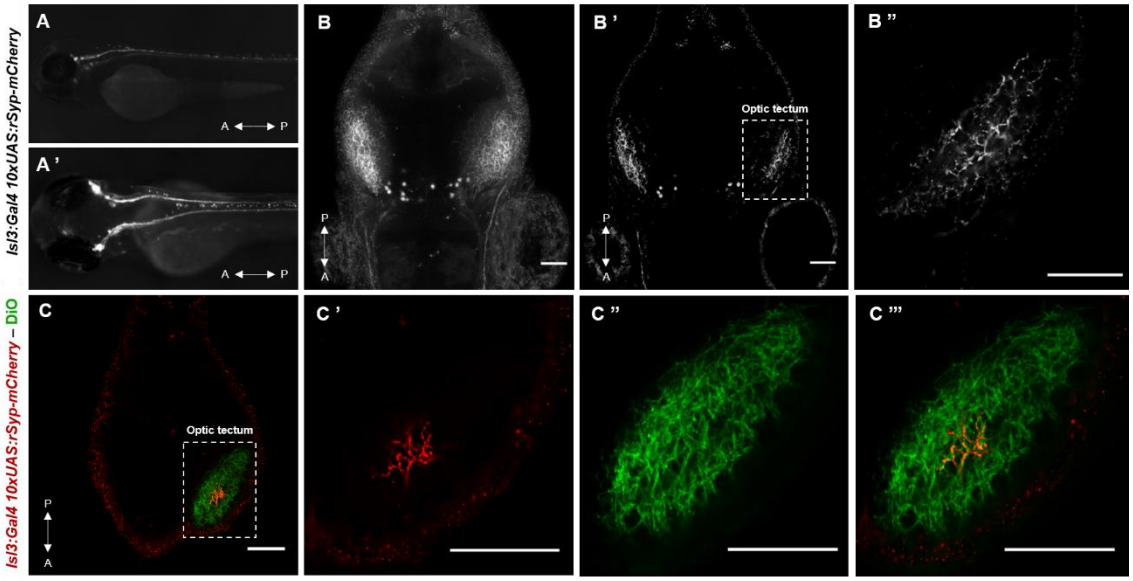

Figure III.13 – *Isl3:Gal4 10xUAS:rSyp-mCherry* transgenic zebrafish line. (A-A') Stereoscope image of a founder zebrafish larva with partial Isl3 expression pattern (only visible the trigeminal nerve expression). Zebrafish larvae was screened for stable expression at 2-3 dpf, using Zeiss StrREO Discovery.V8 scope. Lateral view **(A)**. Dorsal view **(A')**. **(B-B'')** Confocal microscope images of dorsal view of a zebrafish larva brain at 6 dpf. Maximum intensity projection **(B)** and Z-Stack central plane **(B')** of *Isl3:Gal4 10xUAS:rSyp-mCherry* zebrafish brain. The dashed box is shown at higher magnification in **(B'')**. **(C-C''')** Confocal microscope images of dorsal view of a zebrafish larvae brain at 6 dpf with retinotectal projection labeled with DiO (green). The dashed box is shown at higher magnification in C'-C'''. **(C)** Z-stack central plane of *Isl3:Gal4 10xUAS:rSyp-mCherry* zebrafish brain labeled with DiO **(C')** *Isl3:Gal4 10xUAS:rSyp-mcherry* optic tectum nerve terminations (red) **(C'')** DiO labeling the retinal axons that project in optic tectum. **(C''')** Merge of C' and C''. The scale bar indicates 50 µm. A: anterior; P: posterior.

3.2.2. *Isl3:Gal4 10xUAS:rSyp-GCaMP6fEF05* line

From the 36 *Isl3:Gal4 10xUAS:rSyp-GCaMP6fEF05* injected fish that were selected to reach sexual maturity, 29 of them were screened for stable expression. It was estimated that 76% (22/29) of screened fish (Table III.3) contained at least a stable integration of the pTol2-10xUAS:rSyp-GCaMP6fEF05 vector in germ cells, since the progeny exhibited a characteristic Isl3 expression pattern (Figure III.14A-B''). The percentage of stable transgene integration in the screened population varied between 0.60% and 77% (Table III.3). To establish a stable transgenic line, the progeny from zebrafish with lower percentage of stable transgene integration in germ cells was selected to be raised until adulthood.

In order to characterize the fluorescent reporter expression and confirm its correct expression, a small number of F0 positive embryos with 6 dpf was fixed in a PFA solution and imaged at the confocal microscope. As shown in figure III.14 A-B'', the *Isl3:Gal4 10xUAS:rSyp-GCaMP6fEF05* zebrafish line displays a characteristic Isl3 expression pattern with the *isl3* promoter driving GCaMP6fEF05 expression to the cells of trigeminal ganglion, optic tectum and spinal cord.

Like the previous line, in order to confirm the expression of the GCaMP6fEF05 in presynaptic vesicles of the structures labeled by the *isl3* promoter we performed the anterograde labeling of RGCs' axon terminals with the lipophilic dye, DiI (red) (Figure III.14C''). Since the RGC axons are

projected in the optic tectum, it is possible to visualize the synaptic connections (yellow) between their neurons (Figure III.14C'''), which suggest that the expression of GCaMP6fEF05 is being targeted to presynaptic vesicles of cells that correspond to the Isl3 expression pattern.

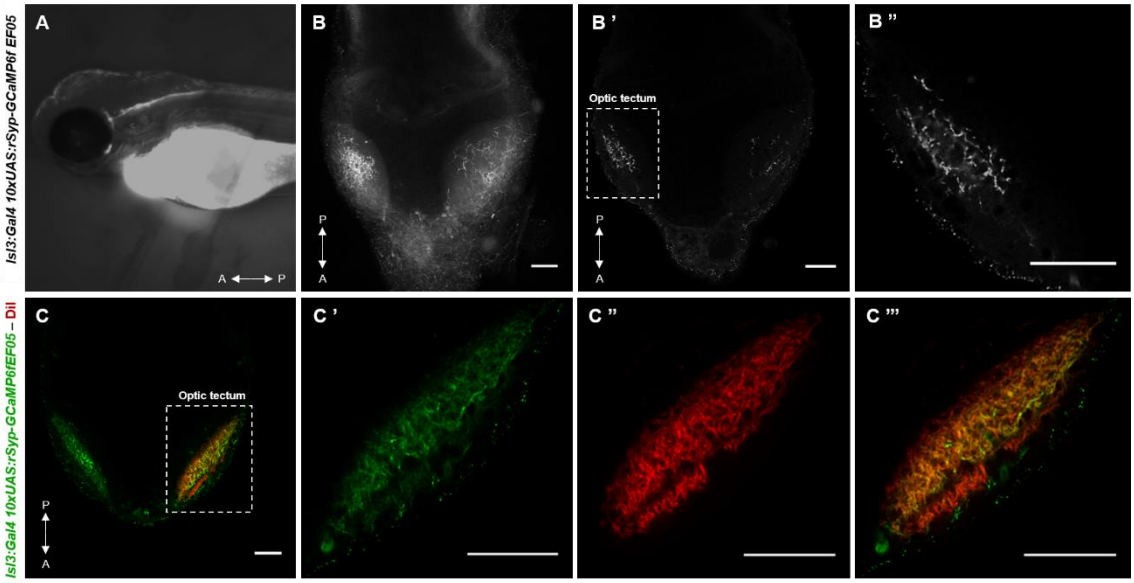

Figure III.14 – *Isl3:Gal4 10xUAS:rSyp-GCaMP6fEF05* transgenic zebrafish line. (A) Stereoscope image of lateral view of a founder zebrafish larva with partial Isl3 expression pattern (only visible the trigeminal nerve expression). Zebrafish larvae were screened for stable expression at 2-3 dpf, using Zeiss StrREO Discovery.V8 scope. **(B-B'')** Confocal microscope images of dorsal view of a zebrafish larva brain at 6 dpf. Maximum intensity projection **(B)** and Z-Stack central plane **(B')** of *Isl3:Gal4 10xUAS:rSyp-GCaMP6fEF05* zebrafish brain. The dashed box is shown at higher magnification in **(B''). (C-C''')** Confocal microscope images of dorsal view of a zebrafish larvae brain at 6 dpf with retinotectal projection labeled with DiI (red). The dashed box is shown at higher magnification in C'-C'''. **(C)** Z-stack central plane of *Isl3:Gal4 10xUAS:rSyp-GCaMP6fEF05* zebrafish brain labeled with DiI **(C')** *Isl3:Gal4 10xUAS:rSyp-GCaMP6fEF05* nerve terminations (green) **(C'')** DiI labeling the retinal axons that project in optic tectum. **(C''')** Merged of C' and C''. The scale bar indicates 50 µm. A: anterior; P: posterior.

3.2.3. *Isl3:Gal4 10xUAS-mScarlet* line

From the 69 *Isl3:Gal4 10xUAS-mScarlet* injected fish that were selected to reach sexual maturity, only 10 of them were screened for stable expression. It was estimated that 60% (6/10) of screened fish (Table III.3) contained at least a stable integration of the pTol2-10xUAS-mScarlet vector in germ cells, since the progeny exhibited a characteristic Isl3 expression pattern (Figure III.15). The percentage of stable transgene integration in the screened population varied between 0.40% and 74% (Table III.3). To establish stable transgenic line, the progeny from zebrafish with lower percentage of stable transgene integration in germ cells was selected to be raised until adulthood.

In order to characterize the fluorescent reporter expression, a small number of F0 positive embryos with 6 dpf was fixed in a PFA solution and imaged at the confocal microscope. As shown in figure III.15, the *Isl3:Gal4 10xUAS-mScarlet* zebrafish line displays a characteristic Isl3 expression pattern with the *isl3* promoter driving mScarlet expression to the cells of trigeminal ganglion, optic tectum, RGCs and spinal cord (Figure III.15A-B'').

We also observed that the *Isl3:Gal4 10xUAS-mScarlet* zebrafish line (Figure III.15A-A') exhibited higher fluorescence intensity than the *Isl3:Gal4 10xUAS:rSyp-mCherry* zebrafish line (Figure III.13A-A').

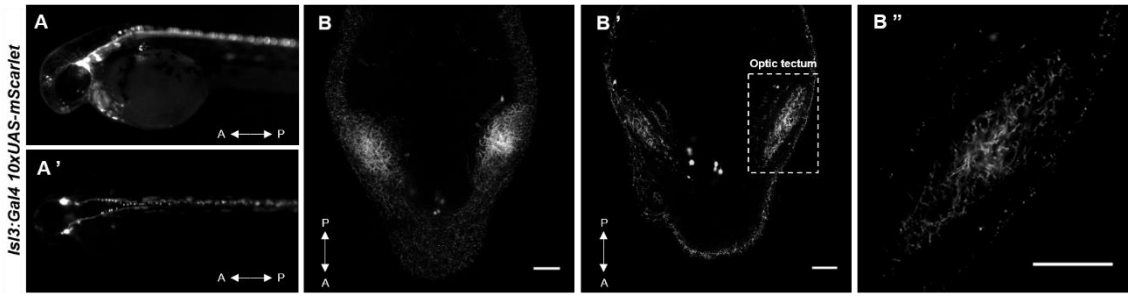

Figure III.15 – ***Isl3:Gal4 10xUAS-mScarlet* transgenic zebrafish line. (A-A')** Stereoscope image of a founder zebrafish larva with partial Isl3 expression pattern (only visible the trigeminal nerve expression). Zebrafish larvae were screened for stable expression at 2-3 dpf, using Zeiss StrREO Discovery.V8 scope. Lateral view **(A)**. Dorsal view **(A')**. **(B-B'')** Confocal microscope images of dorsal view of a zebrafish larva brain at 6 dpf. Maximum intensity projection **(B)** and Z-Stack central plane **(B')** of *Isl3:Gal4 10xUAS-mScarlet* zebrafish brain. The dashed box is shown at higher magnification in **(B'')**. The scale bar indicates 50 µm. A: anterior; P: posterior.

3.2.4. *alpha1Tubulin-mScarlet* line

From the 23 *alpha1Tubulin-mScarlet* injected fish that were selected to reach sexual maturity,17 of them were screened for stable expression. It was estimated that 64% (9/17) of screened fish (Table III.3) contained at least a stable integration of the pTol2-alpha1Tubulin-mScarlet vector in germ cells, since the progeny exhibited a pan-neuronal expression pattern (Figure III.16A-B). The percentage of stable transgene integration in the screened population varied between 0.50% and 61% (Table III.3). To establish a stable transgenic line, the progeny from zebrafish with lower percentage of stable transgene integration in germ cells was selected to be raised until adulthood.

In order to characterize the fluorescent reporter expression, a small number of F0 positive embryos with 6 dpf was fixed in a PFA solution and imaged at the confocal microscope. As shown in the figure III.16A-B, the *alpha1Tubulin-mScarlet* zebrafish line displays a pan-neuronal expression pattern with the *alpha-1-Tubulin* promoter driving mScarlet expression to most neurons throughout the nervous system.

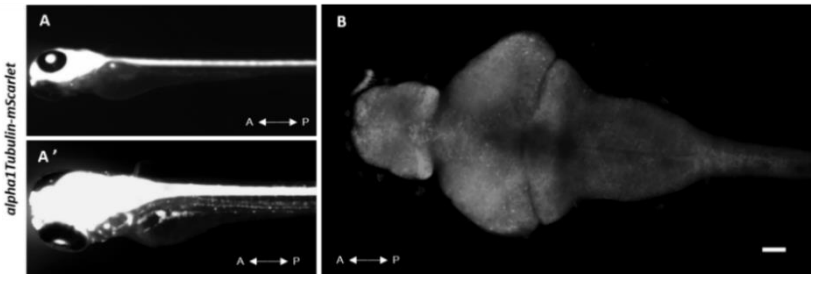

Figure III.16 – *alpha1Tubulin-mScarlet* transgenic zebrafish line. (A-A') Stereoscope image of a founder zebrafish larva with pan-neuronal expression pattern. Zebrafish larvae were screened for stable expression at 2-3 dpf, using Zeiss StrREO Discovery.V8 scope. Lateral view **(A)**. Dorsal view **(A')**. **(B)** Confocal microscope image of dorsal view of a zebrafish larva brain at 6 dpf. Maximum intensity projection. The scale bar indicates 50 µm. A: anterior; P: posterior.

IV. Discussion

The integration of sensory stimuli and their execution in behavioral responses is a dynamic process that involves the communication between large populations of neurons across the whole brain. To understand how the brain produces specific behaviors, it is necessary to identify the neurons and neuronal circuits underlying those behaviors. With the development of state-of-the-art optical techniques and genetic tools, it has been possible to perform whole-brain imaging and to monitor neuronal activity with single-cell resolution and high temporal precision in behaving animals. Thus, the production of whole-brain activity maps is crucial to characterize brain regions and neuronal circuits that mediate motor outputs. Given its favorable features, zebrafish has emerged as a promising model organism in nervous system studies.

In this thesis, recent genetically encoded fluorescent reporters were used to establish new transgenic zebrafish lines, which will be used for studying different populations of neurons and recording neural activity during behavioral responses.

Optimizing state-of-the-art genetic tools for expression in zebrafish

Despite a high number of fluorescent proteins available, several new genetically encoded fluorescent reporters have been developed to improve the fluorophores' characteristics and the fluorescence imaging. In order to generate transgenic zebrafish lines for studying neuronal circuits underlying motor behaviors, UAS and alpha-1-Tubulin expression clones were constructed with the most recent genetically encoded florescent reporter genes: *LSSmOrange* and *mScarlet*.

In order to construct the expression clones, fluorescent reporter genes were isolated from the original vectors by PCR and cloned into a *Tol2* vector (Figure III.2; Figure III.7; Figure III.9). This vector enables the random integration of constructs flanked by the *Tol2* arms in the zebrafish genome, in the presence of transposase. Moreover, when the transgenesis is mediated by the *Tol2* transposon system, the germline transmission frequency is significantly higher than the frequency achieved by any other transgenesis method. Kawakami and co-workers demonstrated that more than 50% of injected zebrafish transmit the transgene insertions to their progeny, when co-injected with transposase mRNA and plasmid DNA with a *Tol2* arms (Kawakami *et al.* 2004). All transgenic lines generated in this work used the *Tol2* transposon system and the results show that more than 50% of injected fish transmitted the transgene insertions to the next generation (Table III.3).

Studies also revealed that transgenic zebrafish created by the *Tol2* transposon system suffer fewer silencing effects after the passage through the generations than transgenic zebrafish created by others transgenesis systems. Transgenic fish created by the non-*Tol2*-DNA microinjection method often carry concatemers of the injected plasmid DNA in the genome, which may contribute to silencing of transgene expression after the passage through the generations.

In contrast, the integration of *Tol2* elements does not cause any gross rearrangement of the surrounding DNA, which allows preserving the transgene expression after F5 generation (Kawakami *et al.* 2000; Kawakami *et al.* 2004; Urasaki *et al.* 2006).

Although the cloning process of pTol2-10xUAS-LSSmOrange and pTol2-alpha1Tubulin-LSSmOrange expression clones is finished, these expression clones were not injected into zebrafish embryos, since the imaging equipment at the Champalimaud Fish Platform did not have a suitable fluorescence filter for emission and excitation of LSSmOrange (excitation/emission at 437/572 nm). Thus, without an appropriate filter it is not possible, at this point, to identify positive larvae after the microinjection.

Generation of transgenic zebrafish lines using the Gal4-UAS transactivation system

The accessibility and optical transparency of zebrafish embryos and larvae make zebrafish a well-suited organism for expressing genetically encoded fluorescent reporters, through transgenic techniques. The transgenic expression in zebrafish is mainly achieved by Gal4-UAS transactivation system. The flexibility to combine several Gal4 driver lines with different UAS reporter lines allows creating multiple transgenic lines that express fluorescent reporters in interesting neuronal populations (Godinho 2011; Rinkwitz *et al.* 2011). In this work, through the use of the Tg (*Isl3:Gal4*$^{+/+}$) driver line (Figure III.11), three transgenic zebrafish lines were generated: *Isl3:Gal4 10xUAS:rSyp-mCherry* (Figure III.13); *Isl3:Gal4 10xUAS:rSyp-GCaMP6fEF05* (Figure III.14) and *Isl3:Gal4 10xUAS-mScarlet* (Figure III.15).

Furthermore, the Gal4-UAS transactivation system makes it possible to enhance gene expression through the number of UAS sequences, since a higher number of UAS sequences leads to an increase of the expression levels of fluorescent reporter genes. However, studies reveal that tandem repetitions of UAS sequences may also be correlated with transcriptional silencing. Each UAS repeat contains a 17 base pairs long CGG-N_{11}-CCG palindromic sequence. The CpG dinucleotides are essential for Gal4 binding, but they are also targets of DNA methylation. When UAS constructs are microinjected into zebrafish embryos, the silencing effects are not present, but when a transgene is stably integrated into the genome, the UAS sequence is prone to CpG methylation, which enables an increase of transcriptional silencing through the generations (Akitake *et al.* 2011; Goll *et al*. 2009).

Constructs with 14xUAS sequences generate higher levels of reporter expression but, on the other hand, are more susceptible to methylation than constructs with 4xUAS sequences (Akitake *et al.* 2011). Thus, in order to balance the efficient expression levels of the fluorescent reporters and minimize the silencing in stable transgenic lines, vectors with 10xUAS sequences were created. The 10xUAS regulatory sequence was available in an entry clone and was efficiently inserted upstream of the fluorescent reporter genes in the *Tol2* destination vectors by LR recombination reaction (Figure III.1; Figure III.4).

Transgenic zebrafish lines for studying neuronal activity and neuronal circuits

Fluorescent calcium indicators can measure neuronal activity. These indicators are capable of reporting sudden changes in intracellular calcium levels in response to an action potential. In the past, fluorescent calcium indicators were commonly applied as synthetic dyes, but their incapacity for targeting specific neuronal cell types led to the use of genetically encoded calcium indicators (GECI) (Higashijima *et al.* 2003; Renninger *et al.* 2011; Scott 2009). These GECIs allow not only the targeting of single neurons and neuronal populations, but also the non-invasive imaging of neuronal activity.

Over the years, several efforts have allowed the optimization of GECIs and, consequently, the creation of improved versions of GCaMPs (Badura *et al.* 2014; Chen *et al.* 2013; Sun *et al*. 2013). The transgenic zebrafish line *Isl3:Gal4 10xUAS:rSyp-GCaMP6fEF05* (Figure III.14), contains an improved version of the original fast GCaMP6. GCaMP6fEF05 was developed by introducing mutations in the EF05 loop domain of the GCaMP6f sequence, through site-directed mutagenesis (Tomás *et al.* unpublished data). The EF05 loop domain mutations were previously described in GCaMP3 (Sun *et al*. 2013). The great advantage of GCaMP6fEF05 is to present a higher signal-to-noise ratio and dynamic range than GCaMP6f. Furthermore, it exhibits comparable kinetics response (Tomás *et al.* unpublished data).

In neurons with higher levels of activity, indicators with fast responses, such as GCaMP6f and GCaMP6fEF05, allow more accurate tracking of changes in firing frequencies. However, the time (~1s) that the cell bodies take to clear calcium is a kinetic limitation in tracking action potential activity. In this situation, Fast-GCaMP's fluorescence signals are limited by the slow time course of calcium changes (Badura *et al.* 2014). Thus, in order to overcome this limitation, GCaMP6fEF05 was fused with the rat synaptophysin tag, which allows directing the expression to presynaptic vesicles. In this case, rSyp is predominantly expressed in presynaptic terminals, where calcium changes are faster than at the cell body. Moreover, when a GECI is directed to synaptic terminals, it also provides a strategy for monitoring neuronal activity at the level of individual synapses.

Synaptophysin is also crucial for studying the connectivity of the neuronal circuits, since it enables the axons' identification (Scott 2009). Although synaptophysin is predominantly expressed in presynaptic terminals, it is also involved in synaptic vesicle exocytosis and endocytosis that occurs along the axons (Meyer & Smith 2006). Therefore, when synaptophysin is fused to a genetically encoded fluorescent reporter, it is possible to identify axons and study axonal arbor growth throughout the zebrafish nervous system. In order to study the connectivity of the neuronal circuits, a *Isl3:Gal4 10xUAS:rSyp-mCherry* zebrafish transgenic line was generated (Figure III.13).

Upon the establishment of synaptic connections, presynaptic vesicles accumulate predominately in presynaptic terminals. Thus, in order to confirm that the fluorescent reporter expression is targeted to these vesicles in the structures labeled by the *isl3* promoter, DiI and DiO lipophilic

dyes were injected into *Isl3:Gal4 10xUAS:rSyp-mCherry* and *Isl3:Gal4 10xUAS:rSyp-GCaMP6fEF05* fixed embryos, respectively. This technique enables the labeling of the entire retinotectal projection and consequently the visualization of the synaptic connections between the RGCs and optic tectum neurons.

Lipophilic dyes dissolve easily into cell membranes. Therefore, when they are injected into the zebrafish eye, DiI and DiO are uptaken by the plasma membrane, labelling the entire retinal ganglion cell axons. Upon projecting into the optic tectum, they form an axonal arbor and establish synaptic connections. Synaptic connections between RGC axons and the optic tectum dendrites lead to the accumulation of presynaptic vesicles in presynaptic terminals of their neurons. Through the use of the dyes, it is possible to observe the colocalization of the RGC's axonal arbor terminals with the genetically encoded rSyp-tag (Figure III.13C'''; Figure III.14C''').

A complementary characterization of lines should be made through the visualization of the optic nerve, since in this structure does not establish synaptic connections. At the confocal microscope, due to the limited depth field, it was not possible to visualize the optic nerve in the preparations. Thus, it would be necessary to perform imaging using a two-photon microscope, since this microscopy enables to obtain in-depth 3D images with high resolution and minimal photo-damage (Renninger & Orger 2013).

Generation of *alpha1Tubulin-mScarlet* transgenic line for studying axonal growth during nervous system development

During the development of the nervous system there is the formation and growth of axons. Axonal growth is required for long distance communication and establishment of connections between cells. One of the proteins identified during this process is the alpha-1-Tubulin (Hieber *et al.* 1998). In order to study axon growth during nervous system development and understand the interactions of neuronal circuits, *alpha-1-Tubulin* expression clones harboring the *alpha-1-Tubulin* putative promoter were generated. This putative promotor includes not only the promoter, but also the first exon and first intron of the *alpha-1-Tubulin* gene, since when it was compared the fish and other species' *alpha-1-Tubulin* genomic region, it was showed regions of conserved DNA in the first exon and first intron. Furthermore, studies also revealed that clones containing the first intron of the *alpha-1-Tubulin* gene lead to higher expression *in vivo* than clones without the first intron (Hieber *et al.* 1998).

In order to generate transgenic zebrafish lines harboring the *alpha-1-Tubulin* putative promoter, *alpha-1-Tubulin* expression clones were first constructed using Gibson Assembly (Figure III.6A; Figure III.7). As this method presents higher efficiency than the classical PCR approach, it was chosen to perform the cloning of the *alpha-1-Tubulin* putative promoter.

In *alpha1Tubulin-mScarlet* transgenic zebrafish line, injected larvae (Figure III.12D) and their progeny (Figure III.16A-A') exhibited a fluorescence intensity significantly higher than the fluorescent intensity exhibited by other generated lines (Figure III.12A-C; Figure III.13A-A'; Figure

III.14A; Figure III.15.A-A'). This can be explained by the pan-neuronal expression pattern, since the *alpha-1-Tubulin* promotor drives the expression throughout the nervous system. In addition, a homogenous expression of mScarlet in transient and stable screens was also observed, which can be explained by direct fusion of the fragments, as a consequence of using Gibson Assembly.

The *alpha-1-Tubulin* putative promoter can also direct the fluorescent reporter expression to the developing neurons through the use of the Gal4-UAS transactivation system. For that, the *alpha-1-Tubulin* putative promoter would have to be cloned into a plasmid with a Gal4FF sequence, in order to create a driver line. The combination of this driver line with different UAS reporter lines, would allow not only the (potential) increase of the expression, but also the creation of zebrafish transgenic lines with different genetically encoded fluorescent reporters without more cloning steps.

Characterization of the expression of the fluorescent reporters in transient and stable expression screens

In order to generate transgenic zebrafish lines, expression clones (Table II.5) were injected in one-cell stage zebrafish embryos. Although all the expression vectors had been injected at the same concentration, 18 ng/µL, a microinjection was previously performed to establish the optimal concentration. This step is very important, since high concentrations lead to a high toxicity and lower concentrations to a lower integration efficiency.

When the screen for transient expression of fluorescent reporter genes was performed, injected larvae with 10xUAS exhibited different levels of brightness and an incomplete Isl3 expression pattern (Figure III.12A-C), which can be explained either by unequal distribution of the microinjected DNA during the embryonic cell divisions (Amsterdam *et al.* 1995) or by the amount of injected DNA, since some injected embryos may have integrated more transgene insertions in their genome than others.

Despite the fact that injected fish exhibit transient expression, they may not transmit the transgene insertions to their progeny. For that to occur, the transgene must be integrated in the germline. When the screen for stable expression was performed, the positive progeny from the injected fish with 10xUAS exhibited a mosaic expression, which suggests evidence of transcriptional silencing caused by the 10xUAS sequences or positional effects (Akitate *et al.* 2011; Roberts *et al.* 2014). Another cause for mosaic expression is the number of insertions integrated in the germline. Injected fish exhibited a variable percentage of stable transgene integration (Table III.3), which means that some zebrafish integrated more copies in germ cells than others. In order to know the exact number of transgene insertions integrated in an individual injected fish, it would be necessary to perform a Southern Blot or a PCR (Kawakami 2005).

In the *Isl3:Gal4 10xUAS-mScarlet* zebrafish line it was also observed that injected larvae (Figure III.12C) and their progeny (Figure III.15A-A') exhibited a higher fluorescence intensity than *Isl3:Gal4 10xUAS-rSyp:mCherry* zebrafish embryos (Figure III.12A; Figure III.13A-A'). This is not

surprising, since Bindels and co-workers reported that mScarlet is about 3.5 times brighter than mCherry. So far, mScarlet is the monomeric red fluorescent protein with the highest brightness (Bindels *et al.* 2017). Another factor that can influence the brightness in *Isl3:Gal4 10xUAS-rSyp:mCherry* is the rSyp tag, since it restricts the mCherry expression to presynaptic vesicles.

V. Conclusion

To understand how neuronal circuits in the brain generate robust and complex behaviors is crucial to identify and characterize specific neurons, as well as to monitor and manipulate neuronal activity throughout the brain. Transgenic zebrafish lines with different genetically encoded fluorescent reporters are constantly being generated for that purpose. The molecular biology tools used nowadays to create these transgenic lines don't rely only in classical cloning techniques or on random DNA insertion after injection. Instead, the smart use of seamless cloning approaches and new cloning systems that allow for a fast pairing of driver and reporter constructs, together with transgenesis mediated by the *Tol2* transposon system has significantly improved the efficacy of zebrafish transgenic generation.

While genetically encoded calcium ion indicators, such as GCaMPs, enable the monitoring of the neuronal activity *in vivo*; fluorescent reporters, such as LSSmOrange and mScarlet, offer unique advantages in fluorescence microscopy imaging, since LSSmOrange enables the multicolor fluorescence microscopy with a single laser wavelength and the mScarlet offers a high brightness. The use of different genetically encoded fluorescent reporters will contribute for a better understanding of the neuronal circuits and their connections, in particular of circuits involved in visual processing during early stages of development. As zebrafish has a visual system that closely resembles the human eye, the study of several visually evoked behaviors in early stages of development enables advancements in the research of vertebrate eye development and disease and visual processing and function.

The generation of new transgenic zebrafish lines and genetic tools allied with the development of sophisticated imaging techniques open up the possibility of whole-brain imaging with high resolution and precision. In the coming years, the challenge will be to combine the approaches developed and currently used in zebrafish to understand how behaviors are generated in higher vertebrates.

VI. References

Abe G, Suster ML, Kawakami K (2016) Tol2-mediated transgenesis, gene trapping, enhancer trapping, and Gal4-UAS system, Third Edit. Elsevier Inc. doi: 10.1016/B978-0-12-374814-0.00002-1.

Ablain J, Zon LI (2013) Of fish and men: Using zebrafish to fight human diseases. Trends Cell Biol 23:584–586. doi: 10.1016/j.tcb.2013.09.009

Akerboom J, Chen T-W, Wardill TJ, et al (2012) Optimization of a GCaMP calcium indicator for neural activity imaging. J Neurosci 32:13819–13840. doi: 10.1523/JNEUROSCI.2601-12.2012

Akerboom J, Carreras Calderón N, Tian L, et al (2013) Genetically encoded calcium indicators for multi-color neural activity imaging and combination with optogenetics. Front Mol Neurosci 6:1–29. doi: 10.3389/fnmol.2013.00002

Akitake CM, Macurak M, Halpern ME, Goll MG (2011) Transgenerational analysis of transcriptional silencing in zebrafish. Dev Biol 352:191–201. doi: 10.1016/j.ydbio.2011.01.002

Amsterdam A, Lin S, Hopkins N (1995) The Aequorea victoria green fluorescent protein can be used as a reporter in live zebrafish embryos. Dev. Biol. 171:123–129

Asakawa K, Kawakami K (2008) Targeted gene expression by the Gal4-UAS system in zebrafish. Dev Growth Differ 50:391–399. doi: 10.1111/j.1440-169X.2008.01044.x

Badura A, Sun XR, Giovannucci A, et al (2014) Fast calcium sensor proteins for monitoring neural activity. Neurophotonics 1:025008. doi: 10.1117/1.NPh.1.2.025008

Bergeler M, Mizuno H, Fron E, Harvey JN (2016) QM/MM-Based calculations of absorption and emission spectra of LSSmOrange variants. J Phys Chem B 120:12454–12465. doi: 10.1021/acs.jpcb.6b09815

Bill BR, Petzold AM, Clark KJ, et al (2009) A primer for morpholino use in zebrafish. Zebrafish 6:69–77. doi: 10.1089/zeb.2008.0555

Bindels DS, Haarbosch L, Van Weeren L, et al (2016) mScarlet: A bright monomeric red fluorescent protein for cellular imaging. Nat Methods 14:53–56. doi: 10.1038/nmeth.4074

Cermak T, Doyle EL, Christian M, et al (2011) Erratum: Efficient design and assembly of custom TALEN and other TAL effector-based constructs for DNA targeting (Nucleic Acids Research (2011) 39 (e82) DOI: 10.1093/nar/gkr218). Nucleic Acids Res 39:7879. doi: 10.1093/nar/gkr739

Chang N, Sun C, Gao L, et al (2013) Genome editing with RNA-guided Cas9 nuclease in Zebrafish embryos. Cell Res 23:465–472. doi: 10.1038/cr.2013.45

Chen TW, Wardill TJ, Sun Y, et al (2013) Ultrasensitive fluorescent proteins for imaging neuronal activity. Nature 499:295–300. doi: 10.1038/nature12354

Chudakov D, Matz M, Lukyanov S, Lukyanov K (2010) Fluorescent proteins and their applications in imaging living cells and tissues. Physiol Rev 90:1103–1163. doi: 10.1152/physrev.00038.2009

Chudakov DM, Lukyanov S, Lukyanov KA (2005) Fluorescent proteins as a toolkit for in vivo imaging. Trends Biotechnol 23:605–613. doi: 10.1016/j.tibtech.2005.10.005

Feierstein CE, Portugues R, Orger MB (2015) Review seeing the whole picture : a comprehensive imaging approach to functional mapping of circuits in behaving. Neuroscience 296:26–38. doi: 10.1016/j.neuroscience.2014.11.046

Fleisch V, Neuhauss SCF (2006) Visual behavior in zebrafish. Zebrafish. 3:191-201. 10.1089/zeb.2006.3.191

Friedrich RW, Genoud C, Wanner AA, et al (2013) Analyzing the structure and function of neuronal circuits in zebrafish. 7:1–8. doi: 10.3389/fncir.2013.00071

Froger A, Hall JE (2007) Transformation of plasmid DNA into E.coli using the heat shock method. J Vis Exp 2007. doi: 10.3791/253

Fron E, De Keersmaecker H, Rocha S, et al (2015) Mechanism behind the Apparent Large Stokes Shift in LSSmOrange Investigated by Time-Resolved Spectroscopy. J Phys Chem B 119:14880–14891. doi: 10.1021/acs.jpcb.5b09189

Giannaccini M, Cuschieri A, Dente L, Raffa V (2014) Non-mammalian vertebrate embryos as models in nanomedicine. Nanomedicine Nanotechnology, Biol Med 10:703–719. doi: 10.1016/j.nano.2013.09.010

Gibson DG, Young L, Chuang RY, et al (2009) Enzymatic assembly of DNA molecules up to several hundred kilobases. Nat Methods 6:343–345. doi: 10.1038/nmeth.1318

Giniger E, Ptashne M (1987) Transcription in yeast activated by a putative amphipathic α helix linked to a DNA binding unit. Nature 330:670–672. doi: 10.1038/330670a0

Godinho L (2011) Live imaging of zebrafish development. Cold Spring Harb Protoc 6:770–777. doi: 10.1101/pdb.top119

Goll MG, Anderson R, Stainier DYR, et al (2009) Transcriptional silencing and reactivation in transgenic zebrafish. Genetics 182:747–755. doi: 10.1534/genetics.109.102079

Gutiérrez-Lovera C, Vázquez-Ríos AJ, Guerra-Varela J, et al (2017) The potential of zebrafish as a model organism for improving the translation of genetic anticancer nanomedicines. Genes (Basel) 8:1–20. doi: 10.3390/genes8120349

Halpern ME, Rhee J, Goll MG, et al (2008) Gal4/UAS transgenic tools and their application to zebrafish. Zebrafish 5:97-110. doi: 10.1089/zeb.2008.0530

Hartley JL, Temple GF, Brasch MA (2000) DNA cloning using in vitro site-specific recombination. Genome Res 10:1788–1795. doi: 10.1101/gr.143000

Hieber V, Dai X, Foreman M, Goldman D (1998) Induction of a1-tubulin gene expression during development and regeneration of the fish central nervous system. J Neurobiol 37:429–440.

Higashijima SI. (2003) Imaging Neuronal Activity During Zebrafish Behavior With a Genetically Encoded Calcium Indicator. J Neurophysiol 90:3986–3997. doi: 10.1152/jn.00576.2003

Higashijima SI (2008) Transgenic zebrafish expressing fluorescent proteins in central nervous system neurons. Dev Growth Differ 50:407–413. doi: 10.1111/j.1440-169X.2008.01023.x

Huang CJ, Tu CT, Hsiao CD, et al (2003) Germ-line transmission of a myocardium-specific GFP transgene reveals critical regulatory elements in the cardiac myosin light chain 2 promoter of zebrafish. Dev Dyn 228:30–40. doi: 10.1002/dvdy.10356

Hutson LD, Campbell DS, Chien C (2004) Analyzing axon guidance in the zebrafish retinotectal System. Cell 76:13–35

Hwang WY, Fu Y, Reyon D, et al (2013) Efficient genome editing in zebrafish using a CRISPR-Cas system. Nat Biotechnol 31:227–229. doi: 10.1038/nbt.2501

Ivics Z, Hackett PB, Plasterk RH, Izsvák Z (1997) Molecular reconstruction of sleeping beauty, a Tc1-like transposon from fish, and its transposition in human cells. Cell 91:501–510. doi: 10.1016/S0092-8674(00)80436-5

Joung JK, Sander JD (2013) TALENs: A widely applicable technology for targeted genome editing. Nat Rev Mol Cell Biol 14:49–55. doi: 10.1038/nrm3486

Kalueff AV, Stewart AM, Gerlai R (2014) Zebrafish as an emerging model for studying complex brain disorders. Trends Pharmacol Sci 35:63–75. doi: 10.1016/j.tips.2013.12.002

Kawakami K, Imanaka K, Itoh M, Taira M (1998) Excision of the Tol2 transposable element of the medaka fish Oryzias latipes in Xenopus laevis and Xenopus tropicalis. Gene 338:93–98. doi: 10.1016/j.gene.2004.05.013

Kawakami K, Shima A (1999) Identification of the Tol2 transposase of the medaka fish Oryzias latipes that catalyzes excision of a nonautonomous Tol2 element in zebrafish Danio rerio. Gene 240:239–244. doi: 10.1016/S0378-1119(99)00444-8

Kawakami K, Shima A, Kawakami N (2000) Identification of a functional transposase of the Tol2 element, an Ac-like element from the Japanese medaka fish, and its transposition in the zebrafish germ lineage. Proc Natl Acad Sci 97:11403–11408. doi: 10.1073/pnas.97.21.11403

Kawakami K, Takeda H, Kawakami N, et al (2004) A Transposon-Mediated Gene Trap Approach Identifies Developmentally Regulated Genes in Zebrafish. Dev Cell 7:133–144

Kawakami K (2005) Transposon tools and methods in zebrafish. Dev Dyn 234:244–254. doi: 10.1002/dvdy.20516

Kawakami K (2007) Tol2: A versatile gene transfer vector in vertebrates. Genome Biol 8:1–10. doi: 10.1186/gb-2007-8-s1-s7

Keegan L, Gill G, Ptashne M (1986) Separation of DNA Binding from the Transcription-Activatng Function of a Eukaryotic Regulatory Protein. Science (80-) 231:699–704

Kikuta H, Kawakami K (2009) Using, stable transgenesis vectors, transposon. Methods Mol Biol 546:. doi: 10.1007/978-1-60327-977-2

Koga A, Suzuki M, Inagaki H, et al (1996) Transposable element in fish. Nature 383:30

Lan CC, Leong IUS, Lai D, Love DR (2011) Disease modeling by gene targeting using microRNAs, Third Edit. Elsevier Inc.

Langheinrich U (2003) Zebrafish: A new model on the pharmaceutical catwalk. BioEssays 25:904–912. doi: 10.1002/bies.10326

Lister J, Robertson C, Lepage T, et al (1999) Nacre encodes a zebrafish microphthalmia-related protein that regulates neural-crest-derived pigment cell fate. Development 126:3757–3767

Ma J, Ptashne M (1987) A new class of yeast transcriptional activators. Cell 51:113–119. doi: 10.1016/0092-8674(87)90015-8

Martins S, Monteiro JF, Vito M, et al (2016) Toward an integrated zebrafish health management program supporting cancer and neuroscience research. Zebrafish 13:S-47-S-55. doi: 10.1089/zeb.2015.1198

Meyer MP (2006) Evidence from in vivo imaging that synaptogenesis guides the growth and branching of axonal arbors by two distinct mechanisms. J Neurosci 26:3604–3614. doi: 10.1523/JNEUROSCI.0223-06.2006

Moens CB, Donn TM, Wolf-Saxon ER, Ma TP (2008) Reverse genetics in zebrafish by TILLING. Briefings Funct Genomics Proteomics 7:454–459. doi: 10.1093/bfgp/eln046

Mosimann C, Zon L (2016) Contemporary zebrafish transgenesis with Tol2 and application for Cre/lox recombination experiments. Methods Cell Biol 104:219–244. doi: 10.1016/bs.mcb.2016.01.009

Nagai T, Sawano A, Park ES, Miyawaki A (2001) Circularly permuted green fluorescent proteins engineered to sense Ca2+. Proc Natl Acad Sci 98:3197–3202. doi: 10.1073/pnas.051636098

Ni Q, Mehta S, Zhang J (2017) Live-cell imaging of cell signaling using genetically encoded fluorescent reporters. FEBS J 285:203–219. doi: 10.1111/febs.14134

Orger MB (2016) Review the cellular organization of zebrafish visuomotor circuits. Curr Biol 26:377–385. doi: 10.1016/j.cub.2016.03.054

Patton EE, Zon LI (2002) The art and design of genetic screens: Drosophila melanogaster. Nat Rev Genet 3:176–88. doi: 10.1038/35103567

Portugues R, Engert F (2009) The neural basis of visual behaviors in the larval zebrafish. Curr Opin Neurobiol 19:644–647. doi: 10.1016/j.conb.2009.10.007

Poulain FE, Gaynes JA, Hörndli CS, et al (2010) Analyzing retinal axon guidance in zebrafish. Methods Cell Biol 100:2–26. doi: 10.1016/B978-0-12-384892-5.00001-3

Prasher DC, Eckenrode VK, Ward WW, et al (1992) Primary structure of the Aequorea victoria green-fluorescent protein. Gene 111:229–233. doi: 10.1016/0378-1119(92)90691-H

Randlett O, Wee CL, Naumann EA, et al. Whole-brain activity mapping onto a zebrafish brain atlas. *Nature methods*. 2015;12(11):1039-1046. doi:10.1038/nmeth.3581

Renninger SL, Schonthaler HB, Neuhauss SCF, Dahm R (2011) Investigating the genetics of visual processing, function and behavior in zebrafish. Neurogenetics 12:97–116. doi: 10.1007/s10048-011-0273-x

Renninger SL, Orger MB (2013) Two-photon imaging of neural population activity in zebrafish. Neurogenetics 62:255–267. doi: 10.1016/j.ymeth.2013.05.016

Rinkwitz S, Mourrain P, Becker TS (2011) Zebrafish: An integrative system for neurogenomics and neurosciences. Prog Neurobiol 93:231–243. doi: 10.1016/j.pneurobio.2010.11.003

Roberts JA, Miguel-Escalada I, Slovik KJ, et al (2014) Targeted transgene integration overcomes variability of position effects in zebrafish. Development 141:715–724. doi: 10.1242/dev.100347

Rodriguez EA, Campbell RE, Lin JY, et al (2017) The growing and glowing toolbox of fluorescent and photoactive proteins. Trends Biochem Sci 42:111–129. doi: 10.1016/j.tibs.2016.09.010

Sadowski I, Ma J, Triezenberg S, Ptashne M (1988) GAL4-VP16 is an unusually potent transcriptional activator. Nature 335:563–564

Santoriello C, Zon LI (2012) Hooked ! Modeling human disease in zebrafish. J Clin Invest 122:2337–2343. doi: 10.1172/JCI60434.combines

Scheer N, Campos-Ortega JA (1999) Use of the Gal4-UAS technique for targeted gene expression in the zebrafish. Mech Dev 80:153–158. doi: 10.1016/S0925-4773(98)00209-3

Scott EK (2009) The Gal4/UAS toolbox in zebrafish: New approaches for defining behavioral circuits. J Neurochem 110:441–456. doi: 10.1111/j.1471-4159.2009.06161.x

Seipel K, Georgiev O, Schaffner W (1992) Different activation domains stimulate transcription from remote ('enhancer') and proximal ('promoter') positions. EMBO J 11:4961–8. doi: 10.1002/J.1460-2075.1992.TB05603.X

Shcherbakova DM, Hink MA, Joosen L, et al (2012) An orange fluorescent protein with a large Stokes shift for single-excitation multicolor FCCS and FRET imaging. Jounal Am Chem Soc 134:7913-23. doi: 10.1021/ja3018972.

Stewart AM, Braubach O, Spitsbergen J, et al (2014) Zebrafish models for translational neuroscience research: From tank to bedside. Trends Neurosci 37:264–278. doi: 10.1016/j.tins.2014.02.011

Stuart GW, McMurray J V, Westerfield M (1988) Replication, integration and stable germ-line transmission of foreign sequences injected into early zebrafish embryos. Development 103:403–12. doi: 10.1242/dev.068080

Sumbre G, de Polavieja GG (2014) The world according to zebrafish: how neural circuits generate behavior. Frontiers in Neural Circuits 8:91. doi: 10.3389/fncir.2014.00091

Sun XR, Badura A, Pacheco DA, et al (2013) Fast GCaMPs for improved tracking of neuronal activity. Nat Commun 4:1–10. doi: 10.1038/ncomms3170

Thermes V, Grabher C, Ristoratore F, et al (2002) I-SceI meganuclease mediates highly efficient transgenesis in fish. Mech Dev 118:91–98. doi: 10.1016/S0925-4773(02)00218-6

Thisse B, Thisse C. (2004) Fast release clones: a high throughput expression analysis. ZFIN Direct Data Submission. (http://zfin.org)

Tomás AR, Renninger S, Royo M, Israely I, Orger M (unpublished data) Cross-species development and validation of genetically. Manuscript in preparation.

Traven A, Jelicic B, Sopta M (2006) Yeast Gal4: A transcriptional paradigm revisited. EMBO Rep 7:496–499. doi: 10.1038/sj.embor.7400679

Urasaki A, Morvan G, Kawakami K (2006) Functional dissection of the Tol2 transposable element identified the minimal cis-sequence and a highly repetitive sequence in the subterminal region essential for transposition. Genetics 174:639–649. doi: 10.1534/genetics.106.060244

Wang K, Ma J, He M, et al (2013) Toxicity assessments of near-infrared upconversion luminescent LaF3: Yb,Er in early development of zebrafish embryos. Theranostics 3:258–266. doi: 10.7150/thno.5701

Weber T, Köster R (2013) Genetic tools for multicolor imaging in zebrafish larvae. Methods 62:279–291. doi: 10.1016/j.ymeth.2013.07.028

Zhang Y, Wiest DL (2016) Using the zebrafish model to study T-Cell Development. Methods Mol Biol 1323:273-292 doi: 10.1007/978-1-4939-2809-5_22

VII. Supplements

Supplement A

Supplement A.1 – Map of the *Tol2* Gateway destination vector.

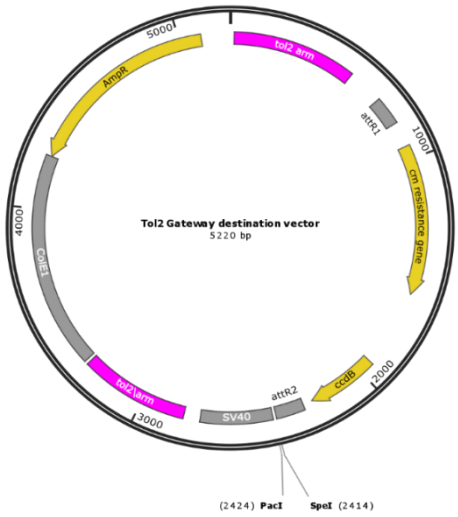

Supplement A.2 – Maps of the pH2B-LSSmOrange (**A**) and pmScarlet_C1 (**B**) vectors.

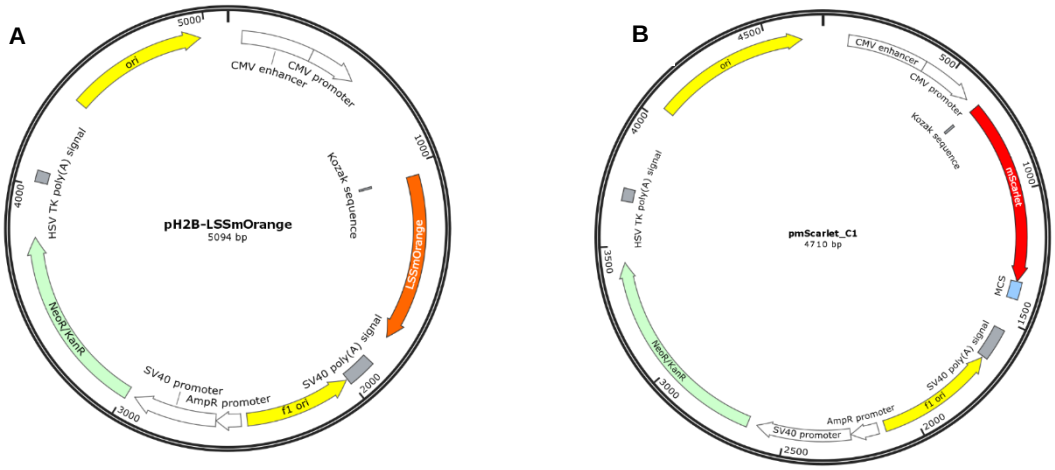

Supplement A.3 – Molecular weight ladder: GeneRuler 1 Kb DNA ladder. Adapted from Thermo Scientific (https://www.thermofisher.com).

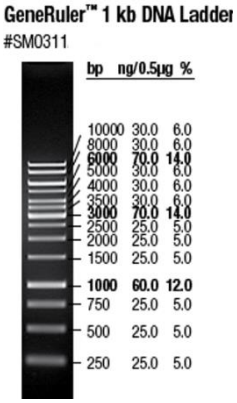

Supplement A.4 - Map of the 10xUAS Entry Clone.

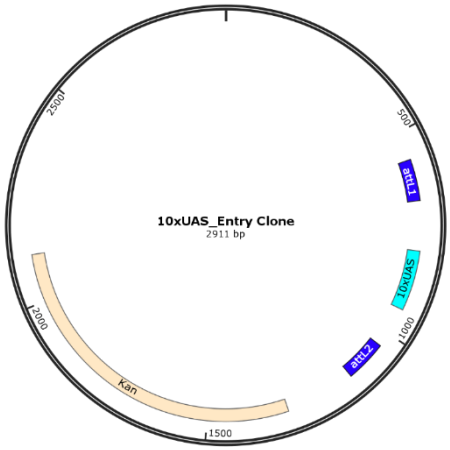

Supplement A.5 – Map of the pT-alpha1Tubulin-GCaMP vector.

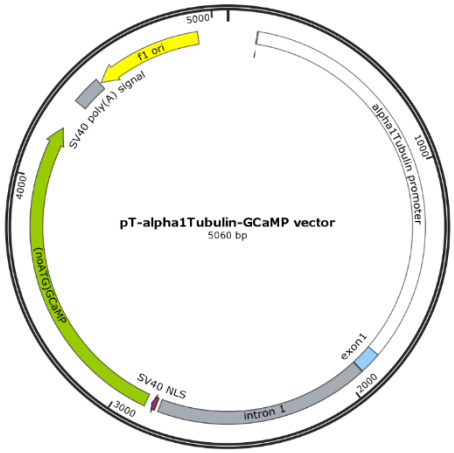

Supplement A.6 – Map of the pCR2.1-TOPO vector.

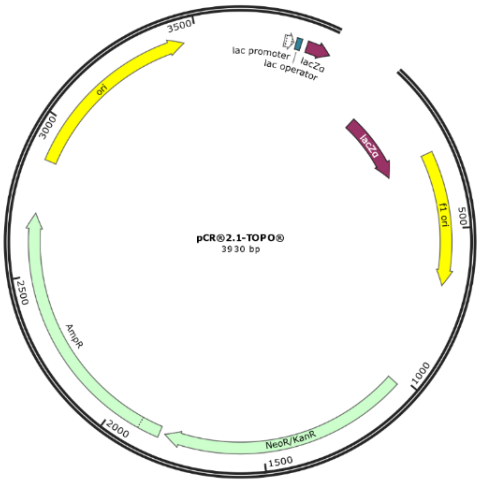

Supplement A.7 – Maps of the pTol2-10xUAS:rSyp-mCherry **(A)** and pTol2-10xUAS:rSyp-GCaMP6fEF05 **(B)** expression clones.

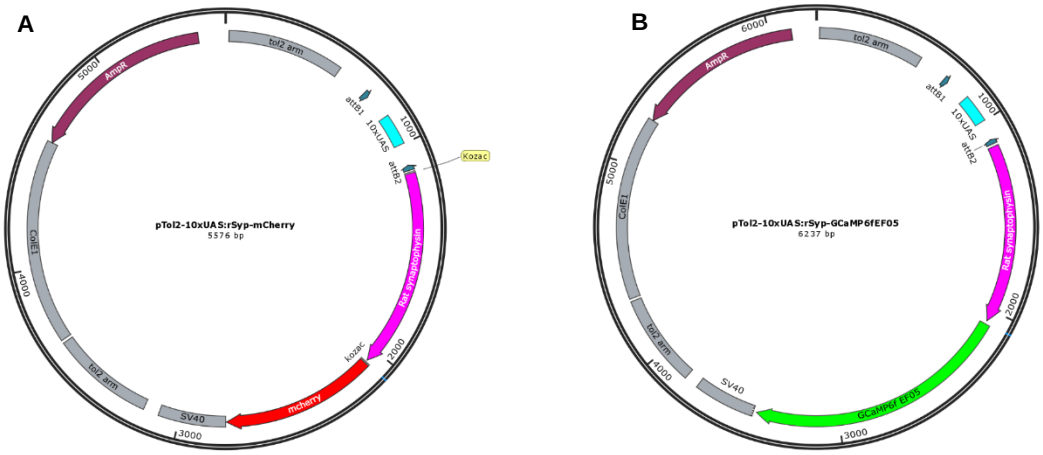

Supplement A.8 – Maps of the pDestTol2-LSSmOrange **(A)** and pDestTol2-mScarlet **(B)** vectors.

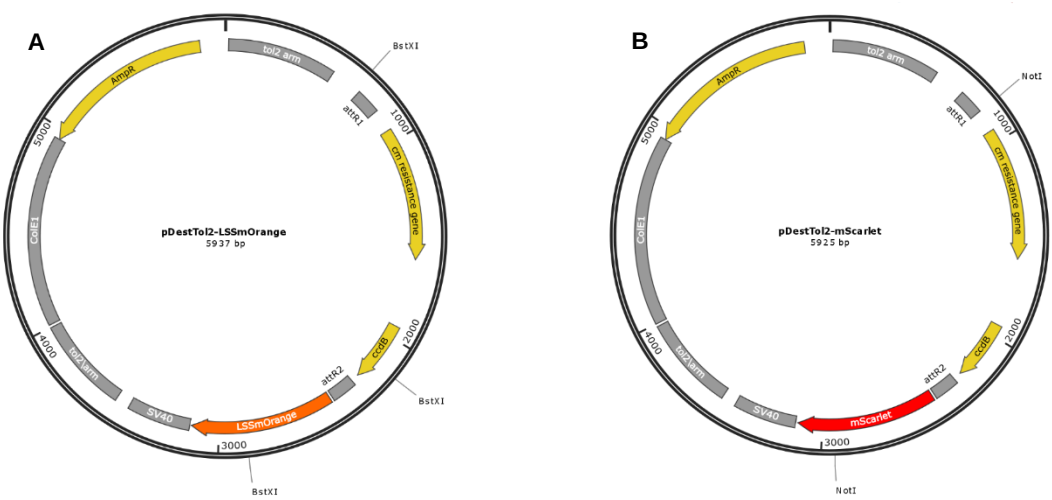

Supplement A.9 – Maps of the pTol2-10xUAS-LSSmOrange **(A)** and pTol2-10xUAS-mScarlet **(B)** expression vectors.

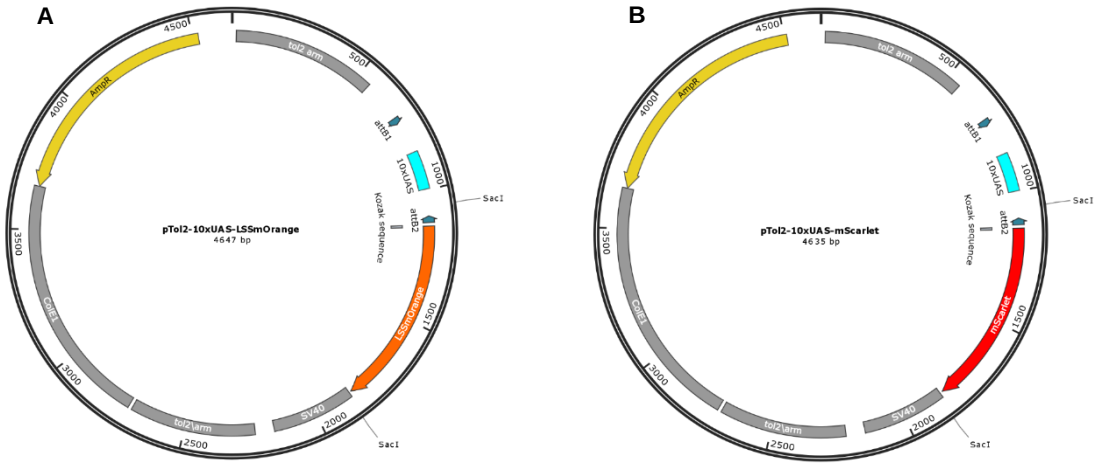

Supplement A.10 – Maps of the pTol2-alpha1Tubulin-LSSmOrange **(A)** and pTol2-alpha1Tubulin-mScarlet **(B)** expression clones.

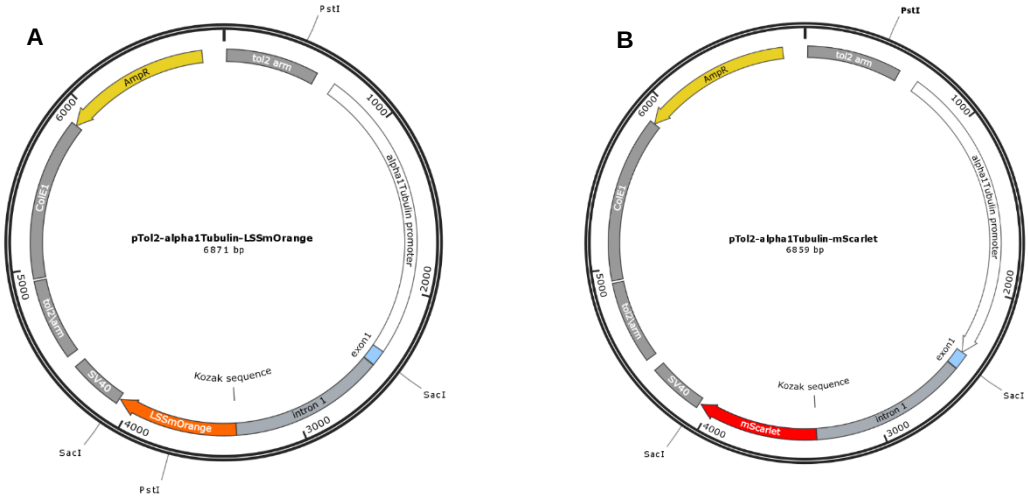

Supplement B

In parallel with the development of the main project, a pet project was initiated:

Characterization of membrane voltage and the effect of membrane voltage-modulator drugs in human cancer cells

I. Introduction

1. Bioelectric signals

Cell behavior is regulated by several intra and extracellular signals. In addition to biochemical gradients, physical forces and transcriptional networks, cell behavior is also regulated by endogenous bioelectrical signals (Levin 2014). These signals are generated and received either by excitable cells or by non-excitable cells. In non-excitable cells, the bioelectrical signals are crucial to control cell functions, such as proliferation, migration, differentiation, cell shape and apoptosis. Furthermore, they are also involved in the regeneration, polarity of whole-body anatomical axes, wound healing and cancer development (Levin 2014; Levin & Stevenson 2012; Yang & Brackenbury 2013).

The bioelectric signals are generated by the movement of ions through ion channels and pumps, which are distributed along the cell membrane. Ions, such as Na^+, K^+, Ca^{2+} and Cl^-, flow across the membrane depending on the selectivity and permeability of each ion channel and pump and the concentration and electric gradients. This leads to an unequal distribution of charges in extra and intracellular medium, generating an electric potential difference, designed by membrane potential (V_m) (Figure I.1) (Levin 2007; Levin 2014; McCaig *et al.* 2005; Yang & Brackenbury 2013).

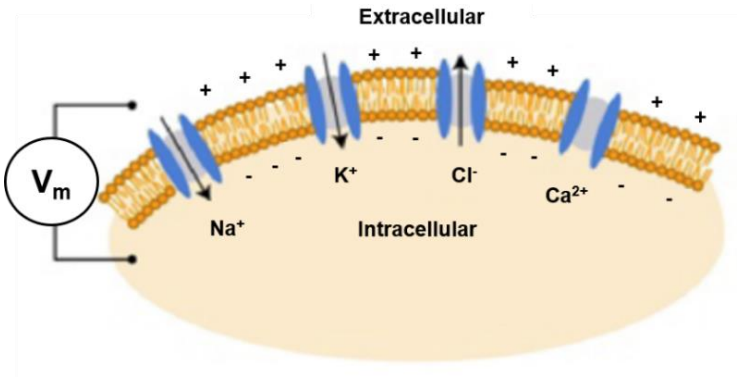

Figure I.1 – Bioelectric signaling at the cell level. The membrane potential is produced by the movement of ions through the ion channels and pumps, that are distributed along the cell membrane. The result is a net negative charge on the inside of the cell relative to the outside. Adapted from Levin 2014.

The cell membrane is typically polarized, since that its inside is more negative compared with its outside (Figure I.1). When the cell is in resting potential, the membrane potential value is approximately – 50 mV. However, this value can be changed by the input or output the charges.

When the input of positive charges or the output of negatives ones occur, the V_m value becomes less negative. This process is commonly known as depolarization. The opposite mechanism is known as hyperpolarization (Levin & Stevenson 2012; Yang & Brackenbury 2013).

2. Membrane potential and cancer

Given the roles of V_m in cell behavior, it is not surprising that the membrane potential is also increasingly involved in the cancer progress (Binggeli & Weinstein 1986; Chernet *et al.* 2016; Prevarskaya *et al.* 2010; Yang & Brackenbury 2013). Studies demonstrate through direct comparation between normal and cancer cells that the resting potential of tumor cells tend to be more depolarized than the resting potential of normal cells (Binggeli & Weinstein 1986; Chernet *et al.* 2016; Yang & Brackenbury 2013). Moreover, tumor cells also exhibit high intracellular Na^+ concentration, which can explain the depolarized phenotype.

In general, cells that are mature, terminally differentiated and quiescent tend to be hyperpolarized, whereas cells with high plasticity, such as embryonic, stem and tumor cells tend to be depolarized (Figure I.2) (Binggeli & Weinstein 1986; Chernet *et al.* 2013; Levin 2014; Levin & Stevenson 2012; Yang & Brackenbury 2013). Thus, the V_m is not only a key mediator of differentiation and proliferation, but also of carcinogenesis.

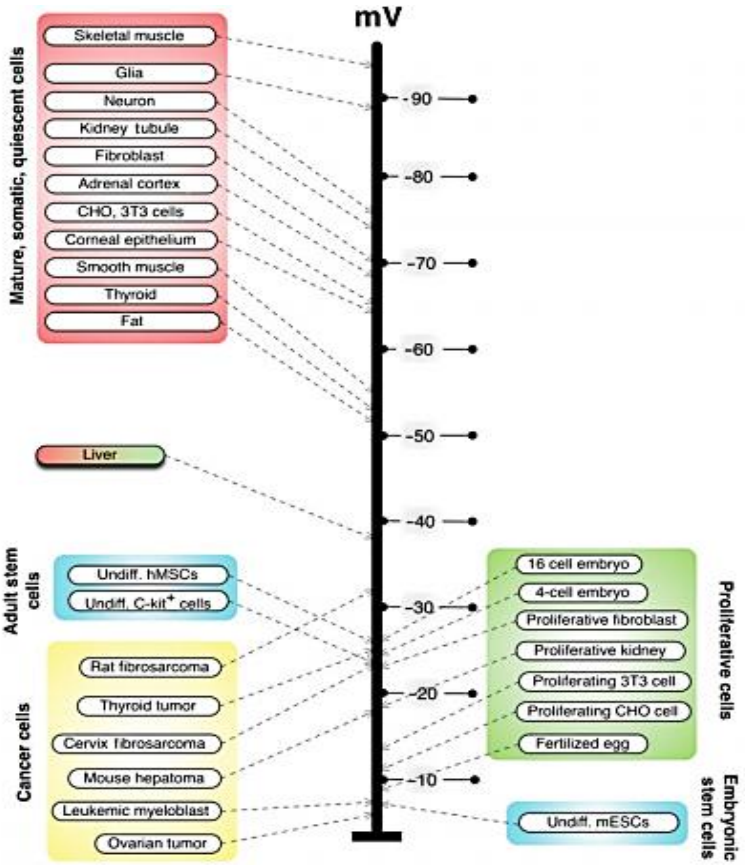

Figure I.2 - Membrane potential scale. Quiescent and terminally differentiated cells tend to be highly polarized, while more plastic cell types: tumor, stem and embryonic cells tend to be depolarized. The mammalian liver has an interesting V_m value, since it is abnormally low for an adult differentiated tissue. This can be correlated with the remarkable regenerative potential of the liver. Adapted from Levin 2012.

Since ion channels and pumps can be involved in ion flux and V_m regulation in cancer cells, anti-cancer studies have focused on Na^+, K^+, Ca^{2+} ions and ion channels as cancer targets and ion channels drugs as a promising class of therapies (Chernet *et al.* 2016; Levin 2014; Yang & Brackenbury 2013).

3. Measuring V_m *in vivo*

The first step to study bioelectric signals is the characterization of the spatiotemporal distributions of ionic parameters *in vivo* and the determination of how they correlate with anatomical and genetic patterning events (Levin & Stevenson 2012). Despite the fact that electrophysiological characteristics of cells can be measured using microelectrodes, several other methodologies have been developed. Nowadays, it is possible to characterize the bioelectrical events through highly sensitive ion-selective extracellular electrode probes (Reid *et al.* 2007), microelectrode arrays (Schonecker *et al.* 2014), individual ion species (Tantama *et al.* 2011; Tseng *et al.* 2010) and voltage-reporting fluorescent dyes, such as CC2-DMPE and $DiBAC_4(3)$ (Adams & Levin 2012a; Adams & Levin 2012b). The fluorescent dyes offer several advantages, such as subcellular resolution, visualization of voltage gradients continuously *in situ*, direct detection of membrane potential overlong time periods independent of cell movements and divisions and ability to measure moving targets (Adams & Levin 2012a; Levin 2014).

4. Aims

As cancer cells exhibit a physiological state more depolarized than differentiated cells, FDA-approved drugs – Barium chloride, Monensin and Gabapentin – were used to study the effect of bioelectric modulation on tumor progression in zebrafish. The study demonstrated that for the same type of cancer, but different cell lines, the same drug can have different effects, which can be explained by different physiological states of tumor cells. Thus, it become necessary to characterize the membrane potential and changes in ion flux of each cell line (Negrão 2017).

The principal aim of this project is to characterize the physiological state of cell membrane of tumor and non-tumor cells lines and understand the true role of the Monensin and Gabapentin in bioelectric modulation of those cell lines.

II. Materials and Methods

1. Cell culture

In order to characterize the physiological state of cell membrane of tumor cells lines, it was used a SW620 cell line (donated by American Type Culture Collection (ATCC)). This is a colon cancer cell line derived from metastatic site, lymph node.

The SW620 cell line was tested for mycoplasma and the handling was performed in a laminar flow hood (Heal Force). The cell counting, cell labeling and light sheet fluorescence microscopy (LSFM) experiments (Lightsheet Z.1, Zeiss) were not performed under aseptic conditions.

1.1. Freeze and thaw of cells

The thawing process started with the removal of the cryovials from liquid nitrogen to a water bath at 37°C for a period of 1-2 minutes. In the laminar flow hood the content of the cryovials was transferred to a falcon, where it was added pre-warmed complete growth medium: Dulbecco's Modified Eagle Medium (DMEM) High Glucose (Biowest) supplemented with 10% fetal bovine serum (FBS) (Sigma) and 1% Penicillin-Streptomycin 10.000 Units/mL (Hyclone). After centrifugation (ORIGEM) of the cell suspension at 1100 rpm for 3 minutes, the cell pellet was resuspended in complete growth medium and transferred into a new sterilized T-flask. The cells were cultured adherently in a humidified atmosphere containing 5% CO_2 at 37°C (inCu Safe).

To maintain a cell line bank, it was necessary, after 2 passages, to freeze the same cell line that had been thawed. For that, the cell pellet was resuspended in 90% FBS with 10% dimethyl sulfoxide (DMSO) (Sigma) and aliquoted in cryovials, that were placed in a - 80°C overnight. In the following day, the cryovials were transferred to a liquid nitrogen tank.

1.2. Cell passage

The SW620 cell line was cultured adherently with complete growth medium in a humidified atmosphere containing 5% CO_2 at 37°C. When the cells achieved a confluence of 70-80%, cell passage was performed. The culture medium was removed from the flask and the cells were washed with 1x Dulbecco's Phosphate Buffered Saline (DPBS) (Gibco, Life Technologies). TrypLE (Gibco, Life Technologies) was added to the flask and incubated at 37°C for 5-10 minutes for cell detachment. To stop the TrypLE action, fresh culture medium was added to the flask and the cell suspension was centrifuged at 1100 rpm for 3 minutes. The supernatant was removed, and the cell pellet was resuspended in complete growth medium. The volume varies with the required dilution factor, that it is commonly adjusted in order to obtain a confluence of 70-80% at the end of about 2-3 days. The cell suspension was added to a new flask with fresh culture medium and cells were incubated in 5% CO_2 at 37°C.

1.3. Cell counting

Before performing the LSFM experiments, it was necessary to obtain an ideal number of cells that should be the same in all experiments. Thus, before the cell labeling, it was performed cell counting in a hemocytometer. Since each of the 4 quadrants have a volume of 0.1mm^3, cell concentration (cells/mL) was calculated according to the following formula:

$$\text{Conc (cells/mL)} = \frac{\text{cell count}}{\text{quadrants number}} \times \text{dilution} \times 10^4 \text{mm}^3\text{mL}^{-1}$$

In the case of the SW620 cell line, it was shown that the ideal number of cells was $2x10^6$ cells, since this number enables the visualization of either single cells or clusters in LSFM experiments.

1.4. Cell labeling

In order to characterize the physiological state of cell membrane of SW620 cells, cell labeling was performed with the voltage-reporting fluorescent dyes: CC2-DMPE and $DiBAC_4(3)$, according to Adams and Levin protocol (Adams & Levin 2012a). Prior to cell labeling, stock solutions of CC2-DMPE (Invitrogen) and $DiBAC_4(3)$ (Invitrogen) fluorescent dyes were prepared according to Adams and Levin protocol (Adams & Levin 2012a), and cells were prepared according to the protocol used for cell passage (Materials and Methods, section 1.2). After cell counting (Materials and Methods, section 1.3), the volume corresponding to the desired number of cells was transferred to an Eppendorf with 1 mL of complete growth medium. Cell labeling was performed in the dark.

2. Light sheet fluorescence microscopy and image analysis

The characterization of the cell membrane's physiological state from the SW620 cell line was attempted using light sheet fluorescence microscopy. The sample was first embedded on low melting agarose (1% (w/v) (Invitrogen) in 1x PBS (composition in table II.1)).

2.1. Sample mounting

After performing cell labeling, cells were resuspended in 100 µL of low melting agarose. Then, the cell suspension was sucked into a capillary (~1 mm) and after the polymerization of the agarose, the embedded sample was pushed out to perform the imaging (Figure II.1). The sample was positioned within a chamber containing an aqueous solution. Depending on the experiment, either 1x PBS or 1x PBS without potassium (composition in table II.1) was used. Since cells were alive, the chamber was heated at 37ºC. Experiments were performed without the control of CO_2.

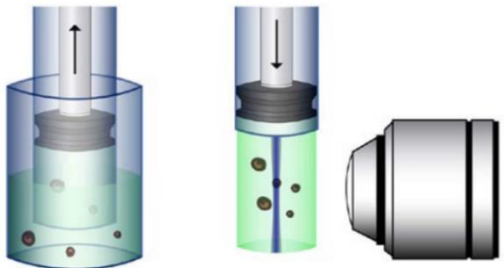

Figure II.1 – Sample mounting. For sample mounting, cells are embedded in 1% low melting agarose and subsequently sucked with a capillary. After the polymerization of the agarose, the embedded sample is pushed out and imaging is performed. Adapted from Flood *et al.* 2013.

2.2. Imaging

For imaging, a 10x illumination objective (N.A 0.2) and a 20x detection objective (N.A 1.0) were used, as well as two lasers: 405 nm (CC2-DMPE) and 488 nm ($DiBAC_4(3)$). Using the ZEN 2010

software, the acquisition parameters (gain, digital gain, digital offset and laser power) were optimized. Cells were imaged in a stack format. All images were analyzed and treated in open source software Fiji. For presentation purposes Z-stack planes were selected.

3. Solutions

Table II.6 – Summary of the composition of solutions used in this work.

Working solutions	Total volume and solvent	Composition
1x PBS	1 L Milli-Q water	1.45 g Na_2HPO_4; 0.24 g KH_2PO_4; 0.2 g KCl; 8 g NaCl
1x PBS without potassium	500 mL Milli-Q water	4.784 g NaCl; 0.8258 g de NaH_2PO_4

III. Results and Discussion

To characterize the physiological state of cell membrane in the SW620 cell line, SW620 cells were labeled with cell-permeable dyes: CC2-DMPE and $DiBAC_4(3)$ voltage-reporting fluorescent dyes. In this experiment, they were used as fluorescence resonance energy transfer (FRET) pairs, in which the CC2-DMPE is the donor and the $DiBAC_4(3)$ is the acceptor. In resting potential, both dyes bind to the outer surface of the cell membrane, which results in efficient FRET. When the cell suffers a membrane potential change, the CC2-DMPE donor remains on the outer surface, but the $DiBAC_4(3)$ mobile acceptor is translocated to closer to or further away from the donor, in proportion to the V_m. In a depolarized state the $DiBAC_4(3)$ acceptor is translocated to further away from the CC2-DMPE donor, which leads to less or no FRET. In a hyperpolarized state, it is the reverse process (Adams & Levin 2012b, Maher *et al.* 2007).

1. Control of the voltage-reporting fluorescent dyes

In order to confirm the functionality of the voltage-reporting fluorescent dyes, imaging was first performed with each dye alone. Since both dyes are cell-permeable, it is expected to observe fluorescence in the cell membrane. As shown in the figure III.1A-B, the fluorescence emitted either by CC2-DMPE or $DiBAC_4(3)$ is mainly present in the cell membrane. This suggests that both dyes are functional.

.

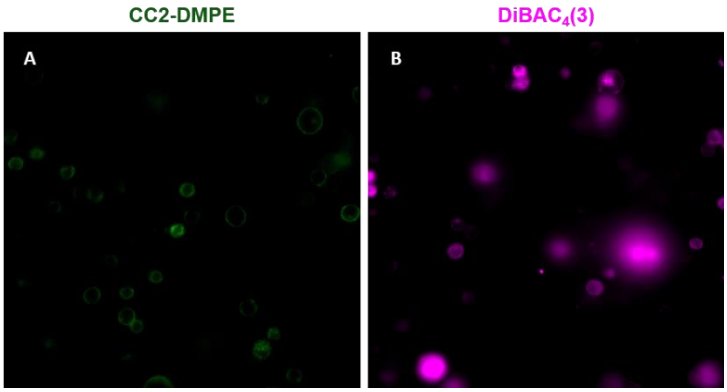

Figure III.1 - Light sheet microscope images of SW620 cells labeled with CC2-DMPE or DiBAC$_4$(3) voltage-reporting fluorescent dyes. (A) Imaging of SW620 cells labeled with the CC2-DMPE donor (green). **(B)** Imaging of SW620 cells labeled with the DiBAC$_4$(3**)** mobile acceptor (magenta). Imaging was performed in 1x PBS.

2. Imaging of SW620 cells with CC2-DMPE and DiBAC$_4$(3) voltage-reporting fluorescent dyes in different conditions

When the cell is depolarized, the CC2-DMPE remains on the outer surface, but the DiBAC$_4$(3) is translocated to the inner surface of the cell membrane, which results in diminished FRET (Adams & Levin 2012b). Since studies reveal that cancer cells tend to be depolarized, it is expected that SW620 cells exhibit a diminished FRET. Thus, in this case, the fluorescence emitted by CC2-DMPE should be significantly lower than the fluorescence emitted by DiBAC$_4$(3).

To characterize the membrane potential of the SW620 cell line, cells were labeled with both voltage-reporting fluorescent dyes and the experiment was performed in 1xPBS. Figure III.2 A-A' shows that the emitted fluorescence by CC2-DMPE and DiBAC$_4$(3) is identical, which means that a diminished FRET is not occurring. Therefore, two hypotheses were suggested: (1) FRET is not taking place or (2) SW620 cells were not depolarized.

In order to study the membrane potential of SW620 cells, the same experiment was performed in 1x PBS without potassium, since this condition causes a membrane polarization. In this case, the DiBAC$_4$(3) is translocated closer to the CC2-DMPE, causing a FRET increase (Adams & Levin 2012b). Thus, in this experiment, the fluorescence emitted by CC2-DMPE must be significantly higher than the fluorescence emitted by DiBAC$_4$(3). Figure III.2B-B' shows the fluorescence emitted by CC2-DMPE and DiBAC$_4$(3) is identical, which means that the membrane potential might not have been changed. Since the effect of bioelectric changes is very fast, this hypothesis is unlikely. Moreover, when the fluorescence emitted by both dyes is compared between experiments (Figure III.2), it is shown that the fluorescence intensity is identical. Thus, this suggests that FRET may not be occurring.

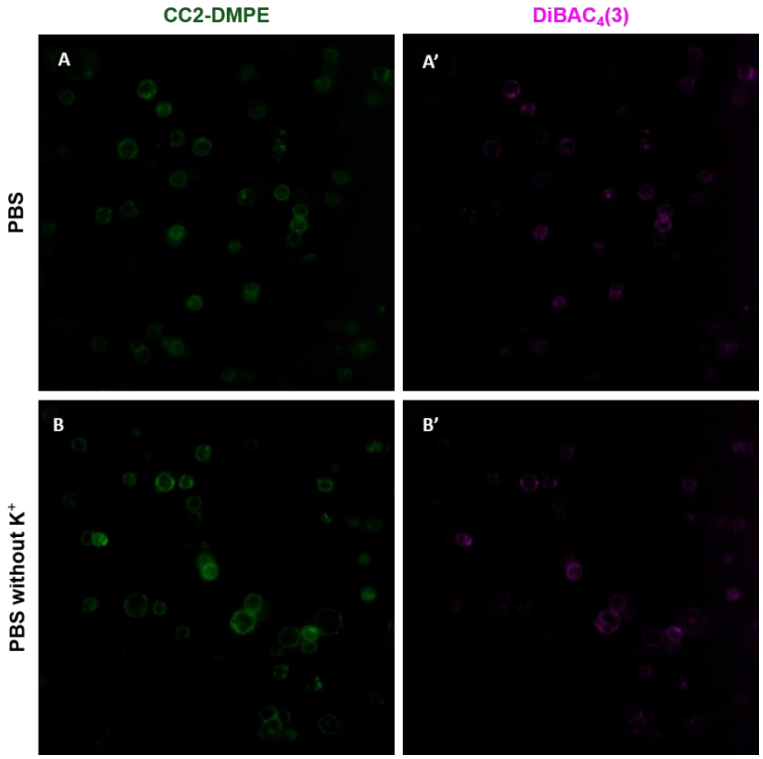

Figure III.2 – Light sheet microscope images of SW620 cells simultaneously labeled with CC2-DMPE or DiBAC$_4$(3) voltage-reporting fluorescent dyes. (A-A') SW620 cells labeled with CC2-DMPE (green) **(A)** and DiBAC$_4$(3) (magenta) **(A')**, when the imaging was performed with 1x PBS. **(B-B')** SW620 cells labeled with CC2-DMPE **(B)** and DiBAC$_4$(3) **(B')**, when the imaging was performed with 1x PBS without potassium (K^+).

The protocol established by Adams and Levin (Adams & Levin 2012a) to measure V_m was designed for ratio imaging. Since Champalimaud Centre for the Unknown does not have at the moment such an available imaging equipment, a new protocol was attempted in a light sheet fluorescence microscope. As *in vitro* cells are not usually studied using LSFM, this approach could also be used to develop a new imaging protocol. However, these experiments were not successful using the dyes as FRET pairs and this type of ratio imaging is not possible in LSFM.

Thus, the next step in this project would be to perform the experiments at the inverted confocal microscope and characterize not only the physiological stage of SW620 cells, but also of other cancer cells and non-cancer cells. Only after studying the physiological stages of different cell lines, would it be possible to design experiments to understand the true effect of Monensin and Gabapentin in the membrane potential.

IV. References

Adams DS, Levin M (2012a) Measuring resting membrane potential using the fluorescent voltage reporters DiBAC4(3) and CC2-DMPE. Cold Spring Harb Protoc 7:459–464. doi: 10.1101/pdb.prot067702

Adams DS, Levin M (2012b) General principles for measuring resting membrane potential and ion concentration using fluorescent bioelectricity reporters. Cold Spring Harb Protoc 7:385–397. doi: 10.1101/pdb.top067710

Binggeli R, Weinstein RC (1986) Membrane potentials and sodium channels: Hypotheses for growth regulation and cancer formation based on changes in sodium channels and gap junctions. J Theor Biol 123:377–401. doi: 10.1016/S0022-5193(86)80209-0

Chernet BT, Adams DS, Lobikin M, Levin M (2016) Use of genetically encoded, light-gated ion translocators to control tumorigenesis. Oncotarget 7:. doi: 10.18632/oncotarget.8036

Chernet BT, Levin M (2013) Transmembrane voltage potential is an essential cellular parameter for the detection and control of tumor development in a Xenopus model. Dis Model Mech 6:595–607. doi: 10.1242/dmm.010835

Flood PM, Kelly R, Gutiérrez-Heredia L, E.G. Reynaud (2013) Sample Preparation. ZEISS Lightsheet Z.1.

Levin M (2007) Large-scale biophysics: ion flows and regeneration. Trends Cell Biol 17:261–270. doi: 10.1016/j.tcb.2007.04.007

Levin M (2012) Molecular bioelectricity in developmental biology: New tools and recent discoveries: Control of cell behavior and pattern formation by transmembrane potential gradients. BioEssays 34:205–217. doi: 10.1002/bies.201100136

Levin M (2014) Molecular bioelectricity: how endogenous voltage potentials control cell behavior and instruct pattern regulation in vivo. Mol Biol Cell 25:3835–3850. doi: 10.1091/mbc.E13-12-0708

Levin M, Stevenson CG (2012) Regulation of cell behavior and tissue patterning by bioelectrical signals: challenges and opportunities for biomedical engineering. Annu Rev Biomed Eng 14:295–323. doi: 10.1146/annurev-bioeng-071811-150114

Maher MP, Wu NT, Ao H (2007) pH-insensitive FRET voltage dyes. J Biomol Screen 12:656–667. doi: 10.1177/1087057107302113

McCaig CD (2005) Controlling cell behavior electrically: current views and future potential. Physiol Rev 85:943–978. doi: 10.1152/physrev.00020.2004

Negrão M (2017) The effect of bioelectrical modulators on tumor progression. Master thesis. Faculdade de Ciências e Tecnologia, Universidade Nova de Lisboa.

Prevarskaya N, Skryma R, Shuba Y (2010) Ion channels and the hallmarks of cancer. Trends Mol Med 16:107–121. doi: 10.1016/j.molmed.2010.01.005

Schönecker S, Kraushaar U, Düfer M, et al (2014) Long-term culture and functionality of pancreatic islets monitored using microelectrode arrays. Integr Biol (United Kingdom) 6:540–544. doi: 10.1039/c3ib40261d

Tantama M, Hung YP, Yellen G (2011) Imaging intracellular pH in live cells with a genetically encoded red fluorescent protein sensor. J Am Chem Soc 133:10034–10037. doi: 10.1021/ja202902d

Tseng A-S, Beane WS, Lemire JM, et al (2010) Induction of vertebrate regeneration by a transient sodium current. J Neurosci 30:13192–13200. doi: 10.1523/JNEUROSCI.3315-10.2010

Yang M, Brackenbury WJ (2013) Membrane potential and cancer progression. Front Physiol 4 JUL:1–10. doi: 10.3389/fphys.2013.00185